Near-surface hydraulic conductivity of Northern Hemisphere glaciers

Stevens, Ian Thomas; Irvine-Fynn, Tristram; Porter, Philip R.; Cook, Joseph M.; Edwards, Arwyn; Smart, Martin; Moorman, Brian J.; Hodson, Andrew J.; Mitchell, Andrew

Published in:
Hydrological Processes

DOI:
10.1002/hyp.11439

Publication date:
2018

Citation for published version (APA):
Stevens, I. T., Irvine-Fynn, T., Porter, P. R., Cook, J. M., Edwards, A., Smart, M., Moorman, B. J., Hodson, A. J., & Mitchell, A. (2018). Near-surface hydraulic conductivity of Northern Hemisphere glaciers. *Hydrological Processes*, *32*(7), 850-865. https://doi.org/10.1002/hyp.11439

Near-surface hydraulic conductivity of Northern Hemisphere glaciers

Ian T. Stevens[1], Tristram D.L. Irvine-Fynn[1]*, Philip R. Porter[2], Joseph M. Cook[3], Arwyn Edwards[1,4], Martin Smart[2], Brian J. Moorman[5], Andy J. Hodson[3,6], Andrew C. Mitchell[1]

[1]Centre for Glaciology, Aberystwyth University, Aberystwyth, UK
[2]Geography and Environmental Science, University of Hertfordshire, Hatfield, UK
[3]Department of Geography, University of Sheffield, Sheffield, UK
[4]Institute of Biology Environment Rural Science, Aberystwyth University, Aberystwyth, UK
[5]Department of Geography, University of Calgary, Alberta, Canada
[6]UNIS, Longyearbyen, Norway

* Communicating author: tdi@aber.ac.uk

Abstract

The hydrology of near-surface glacier ice remains a neglected aspect of glacier hydrology despite its role in modulating meltwater delivery to downstream environments. To elucidate the hydrological characteristics of this near-surface glacial "weathering crust", we describe the design and operation of a bespoke capacitance-based piezometer that enables rapid, economical deployment across multiple sites and provides an accurate, high-resolution record of near-surface water level fluctuations. Piezometers were employed at ten northern hemisphere glaciers, and through the application of standard bail-recharge techniques, we derive hydraulic conductivity (*K*) values from 0.003 to 3.519 m d^{-1}, with a mean of 0.185 ± 0.019 m d^{-1}. These results are comparable to those obtained in other discrete studies of glacier near-surface ice, and for firn, and indicate that the weathering crust represents a hydrologically inefficient aquifer. Hydraulic conductivity correlated positively with water table height but negatively with altitude and cumulative short-wave radiation since the last synoptic period of either negative air temperatures or turbulent energy flux dominance. The large range of *K* observed suggests complex interactions between meteorological influences and

This article has been accepted for publication and undergone full peer review but has not been through the copyediting, typesetting, pagination and proofreading process which may lead to differences between this version and the Version of Record. Please cite this article as doi: 10.1002/hyp.11439

differences arising from variability in ice structure and crystallography. Our data demonstrate a greater complexity of near-surface ice hydrology than hitherto appreciated, and support the notion that the weathering crust can regulate the supraglacial discharge response to melt production. The conductivities reported here, coupled with typical supraglacial channel spacing, suggest that meltwater can be retained within the weathering crust for at least several days. This has implications not only for the accuracy of predictive meltwater runoff models, but we also argue for biogeochemical processes and transfers that are strongly conditioned by water residence time and the efficacy of the cascade of sediments, contaminants, microbes and nutrients to downstream ecosystems. Since continued atmospheric warming will incur rising snowline elevations and glacier thinning, the supraglacial hydrological system may assume greater importance in many mountainous regions and, consequently, detailing weathering crust hydraulics represents a research priority since the flow-path it represents remains poorly constrained.

Keywords: Piezometer, Supraglacial Ecosystem, Weathering Crust, Hydraulic Conductivity, Near-surface Ice, Aquifer, Bail-recharge, Turbulent Energy Fluxes.

1. Introduction

Most glacial runoff occurs during the summer melt season and typically fluctuates according to diurnal energy balance oscillations (Hock *et al.*, 2005). It has often been assumed that the snow-free glacier surface imparts minimal delay between meltwater generation and its delivery to englacial, subglacial and proglacial environments (e.g. Fountain and Walder, 1998). However, meltwater storage at an ablating glacier surface has been inferred from geophysical data (e.g. Irvine-Fynn *et al.*, 2006, Moore *et al.*, 1999) and meltwater budgets (e.g. Irvine-Fynn, 2008; Larson, 1978; Smith *et al.*, 2017). Discrepancies in the timing and volume of modelled ablation and observed meltwater discharge have also been observed for snow-free supraglacial catchments in alpine (e.g. Munro, 2011) and ice sheet (e.g. McGrath*, et al.*, 2011, Rennermalm*, et al.*, 2013; Smith *et al.*, 2017) settings. Consequently, there has been a growing recognition of the glacial "weathering crust" (Muller & Keeler, 1969): the shallow (typically 0.01 - 2 m) layer of porous ice which typifies ablating glacier surfaces, which has been referred to as "honeycomb" or "coral" ice (e.g. Cutler and Munro, 1996; Zeng *et al.*, 1984). Despite the recent surge in interest in supraglacial hydrology evident in the literature, (e.g. Gleason *et al.*, 2016; Karlstrom *et al.*, 2013, 2014; Mantelli *et al.*, 2015; McGrath *et al.*, 2011; Rippin *et al.*, 2015; Smith*, et al.* 2015; St. Germain and Moorman, 2016; Yang *et al.*, 2016; Yang and Smith, 2013), a detailed

understanding of the hydraulic conductivity (K) and permeability (κ) of the weathering crust, and their variation in space and time is still lacking (Irvine-Fynn *et al.*, 2011a; Karlstrom *et al.*, 2014; Cook *et al*., 2016a).

The porous weathering crust ice layer develops as a function of three primary drivers: (i) subsurface melt caused by incident solar radiation (Müller and Keeler, 1969; Munro, 1990); (ii) heat flow within interstitial spaces that further contributes to declining ice crystal cohesion (Hoffman *et al.*, 2014; Mader, 1992; Nye, 1991), and (iii) kinetic energy and frictional heat transfers from water flow through interstitial flowpaths (Koizumi and Naruse, 1994). The depth of the weathering crust that develops during synoptic clear sky conditions is related to Beer's Law (Cook *et al.*, 2016a; Oke, 1987), which defines an exponential increase in bulk ice density with depth (LaChapelle, 1959) from ~300-400 kg m^{-3} to 870-917 kg m^{-3} over length scales between a few centimetres to several decimetres or more (Brandt and Warren, 1993; Müller and Keeler, 1969; Schuster, 2001; Shumskii, 1964; Smith *et al*., 2017). Factors controlling the depth of weathering crust development include the coefficient of extinction of shortwave radiation (SWR_{in}), itself governed by ice type, crystal size, impurity and air bubble content and their emergence rates, and the zenith angle, intensity and duration of solar radiation receipt. Clear skies lead to glacier surface energy balance dominated by radiative fluxes, which promote weathering crust growth, in some cases of stagnating ice to a depth in excess of 2 m (Fountain and Walder, 1998; Larson, 1977). Reduced incident radiation (e.g. due to cloud cover) and high precipitation cause turbulent energy to dominate the glacier surface energy balance, promoting surface lowering which reduces the thickness of the weathering crust (Müller and Keeler, 1969; Shumskii, 1964). Variations in the thickness and porosity of the weathering crust at synoptic and seasonal time-scales likely results lead to temporal and spatial variability in supraglacial hydraulic permeability, conductivity and meltwater storage potential. The dynamic properties of this near-surface porous media likely influence meltwater transfer, modulating the lag time between *in situ* meltwater production and associated runoff signals (Karlstrom et al., 2014; Munro, 2011; Smith *et al*., 2017).

Hydraulic conductivities between 10^{-2} and 10^{-6} m s^{-1} (10^{3} and 10^{-2} m d^{-1}) for differing depths, sample times and general surface topographies have previously been measured for glaciers in Alaska and Norway (Larson, 1977; Theakstone and Knudsen, 1981; Wakahama, 1978; Wakahama*, et al.*, 1973). In contrast, theoretical estimates based on assumed values for near-surface ice properties suggest a permeability of ~10^{-10} m^2 for the Llwellyn Glacier, Juneau Ice Field, Canada (Karlstrom *et al.*, 2014). However, as Theakstone and Knudsen (1981) cautioned, rigorous comparisons of these types of data should not be made, due to marked contrasts in geographical location, climatic setting, glacier

morphology, and experimental methods. Rather, these limited observations emphasise the need to use a standardised approach to characterising glacier surface hydraulic conductivity across a range of study areas to understand the processes controlling shallow-subsurface glacier hydrology.

In addition to controlling and modulating meltwater fluxes, the importance of weathering crust hydrology is of primary concern for understanding ice surface nutrient and sediment fluxes and supraglacial microbial ecology. Redistribution of fine supraglacial debris and dust across an ablating ice surface is commonly described (e.g. Adhikary *et al*., 2000; Hodson *et al*., 2007; Oerlemans *et al*., 2009*;* Porter *et al*., 2010; Irvine-Fynn *et al*., 2011b), while hydrological flowpaths in the glacier near-surface control the export of microbes and associated nutrients to extraglacial environments (Cook *et al.*, 2016a; Irvine-Fynn *et al.*, 2012; Hotaling *et al*., 2017). The weathering crust is now recognised as an ecosystem in its own right (e.g. Hodson *et al*., 2008; Stibal *et al.*, 2012; Irvine-Fynn and Edwards, 2014; Cook *et al.*, 2016a, 2016b). The hydrological characteristics of the weathering crust influence microbial activity in cryoconite (Edwards *et al.*, 2011; Hodson *et al.*, 2007) and the increased residence time afforded by percolation within the interstitial voids of the weathering crust affords microbiota, fine inorganic and organic particles, dissolved nutrients and viruses opportunities for interaction and turnover in spite of the low growth rates and metabolic activities associated with cold environments (Rassner *et al*., 2016). Furthermore, legacy contaminant and particulate impurity transport through glacier systems (e.g. Bogdal et al., 2009; Hodson, 2014; Lokas *et al*., 2016) and their accumulation in down-stream environments (e.g. Bettinetti *et al.*, 2016; Bizzotto *et al*., 2009; Bogdal *et al.*, 2010) must be influenced by hydrological flow through the porous near-surface ice – a process which remains a contemporary research imperative (Grannas*, et al.*, 2013). For these reasons, with recognition of understanding the hydraulic conductivity of the weathering crust assumes significance in the hydrology, biogeochemistry, ecotoxicology and ecology of supraglacial systems.

Therefore, to address the critical research gap weathering crust hydrological characteristics represent, we undertook the first multi-site study to assess hydraulic conductivity using a consistent methodology adapted from terrestrial hydrology. Traditional terrestrial hydrological techniques developed for groundwater investigations can be applied to glacial environments (e.g. Derikx, 1973; Sharp*, et al.*, 1998). Soil and bedrock aquifers are porous media with a depth-limited storage capacity, making their measurement techniques transferable to the analogous supraglacial weathering crust (Hodgkins, 1997; Irvine-Fynn and Edwards, 2014; Lliboutry, 1996; Nye, 1991). A novel electronic piezometer was used to monitor water levels and recharge rates in auger holes at high temporal resolution to derive hydraulic conductivity (*K*) values. We describe the findings from eight valley glaciers distributed across the Northern Hemisphere, and two sites at the western margin of the

Greenland Ice Sheet, and elucidate potential drivers of weathering crust development and hydraulic properties.

2. Materials and methods:

To examine the hydraulic conductivity, *K*, of the glacial weathering crust we employed piezometer-based techniques adapted from those used to measure groundwater transfers (Freeze and Cherry, 1979; Amoozegar and Warwick, 1996). Recently, a similar approach has been used to examine the firn aquifer on the Greenland Ice Sheet (see Miller *et al.*, 2017).

2.1 Electronic piezometer design

Capacitance piezometers have been well-described in the literature (e.g. Wilner, 1960; Ross, 1983; Baxter 1996; Reverter *et al*., 2005). Here, a complementary metal-oxide semiconductor (CMOS) device (e.g. Texas Instruments, USA item TLC555CP) was configured in a circuit that acts as an oscillator with an output frequency determined by the capacitance of capacitor C1 and the resistance of resistor R2 (Figure 1a, Figure 1c). The capacitor was created using a 0.6 m length of 50 mm polypropylene tubing inside which was placed a 50 cm length of 1 mm aluminium angle and a looped 0.25 mm (30 AWG) Kynar insulated silver-plated copper wire (Figure 1b). The Kynar wire is kept taut by anchoring the wire with a 3 mm nylon bolt at the top of the aluminium angle, and with a 25 mm × 4 mm stainless steel extension spring secured with a nylon bolt at the base of the aluminim angle (see also Ross, 1983). Regular holes are drilled around the circumference of the tube along its length, to allow uninterupted ingress and egress of water. The frequency of the output signal scales in proportion to capacitance; as the water level rises capacitance is reduced, output frequency increases and *vice versa*. To reduce heat transfer between the device and ice surface, tubes are coated in adhesive silver foil. This foil cover was found to reduce the exposed tube temperatures by 0.5 °C when subjected to typical mountain environment conditions. The addition of a frequency to voltage convertor (e.g. Texas Instruments, USA LM2907N) produces a single-ended voltage output of between 1.0 and 2.8 V which, here, is logged using a self-powered USB 'Track-it' Data Logger (Monarch Instruments, USA). The circuitry and battery are housed at the top of the piezometer within the plastic tube and require minimal weatherproofing. The design of the circuit means that output frequency is independent of supply voltage, therefore there is negligible variation to the output signal due to battery depletion, making the sensors well suited to deployment in remote environments where regular battery changes may not be possible. Piezometer output is close to linear (Figure 1d-f) and is not influenced by electrical conducitivity (EC), suspended sediment concentration (SSC) or temperature levels within the limits commonly observed in supraglacial environments. Calibration of individual piezeometers is

simply a matter of recording voltage at a variety of known, incremental water levels and applying a linear function to the resultant datesets.

2.2 Electronic piezometers: data processing

Aquifer hydraulic conductivity (*K*) is commonly assessed using piezometer tests, which quantify the nature of hydrological recovery of an auger hole following a disturbance to the water level, either where auger holes are emptied (bail test) or artificially overfilled (slug test) (Amoozegar and Warwick, 1986; Moore, 2002; Freeze and Cherry, 1979). A notable issue with the application of slug testing in the glacial environment is caused by the low permeability (e.g. Lliboutry, 1971, Lliboutry, 1996, Nye, 1991) and density gradient (e.g. Muller and Keeler, 1969) of ice when compared with a soil aquifer for which the test was designed. By introducing additional water to an auger-hole, the water table would artificially rise and water would flow through the unsaturated, higher porosity weathering crust, and likely result in an overestimation of *in situ K*. The bail-recharge method was considered more appropriate for use in the supraglacial environment, although water flow into the auger-hole occurs isotropically from three-dimensions as a 'false' water head is generated by the empty hole (Figure 2; Moore, 2002). However, by considering the rate of water level rise, this phenomenon can be eliminated mathematically with several solutions proposed, including the formulation by Bouwer and Rice (1976):

$$K = \frac{Q \cdot \ln(\frac{R_e}{r_w})}{2\pi \cdot L \cdot y} \qquad \text{Eq.1}$$

where *Q* is the water flow into the auger-hole ($cm^3\ s^{-1}$), and the remaining length terms (all in cm) include *L,* the height of the well through which water enters, *y* is the vertical distance between the water surface in the auger hole and the equilibrium water table, R_e is the effective radius over which *y* is dissipated, and r_w is the radius of the auger-hole. For the equation to be valid, a single auger-hole is required and it is specifically applicable to partially penetrating, unsealed wells in unconfined aquifers, such as the weathering crust. *Q* can be defined through knowledge of the auger-hole dimensions and the recharge rate detailed in the output from the piezometer as the water level recovers. Whilst R_e can be determined empirically using axisymmetric node networks (Bouwer and Rice, 1976), the term $\ln(R_e/r_w)$ can be determined using an approximation given as:

$$\ln\left(\frac{R_e}{r_w}\right) = \left[\frac{1.1}{\ln(\frac{h}{r_w})} + \frac{A+B \cdot \ln[(D-h)/r_w]}{L/r_w}\right]^{-1} \qquad \text{Eq.2}$$

for which *D* is the distance between the water table in the aquifer and the impermeable ice representing the base of the aquifer, and *h* the depth of the water in the auger hole (both in cm). *A* and *B* are dimensionless constants, determined using the ratio L/r_w (see Bouwer and Rice, 1976). One condition of the empirical approximation presented in Equation 4 is that $0 < (D-h)/r_w \leq 6$; if these conditions are not met, $(D-h)/r_w$ is adjusted to equal 6.

Following the derivation of *K*, primary ice permeability (κ) can be calculated, after Bear (1972):

$$\kappa = K\frac{\mu}{\rho_w g} \qquad \text{Eq.3}$$

where ρ_w is the density of water (taken as 1000 kg m^{-3}), *g* is acceleration due to gravity (0.981 m s^{-2}) and μ is the dynamic viscosity of water (in Pa S). Water viscosity is temperature dependent (Figure 3) and, in the range of interest characteristic for supraglacial water temperatures (< 2 °C; Isenko et al (2005)) it is useful to note that viscosities are 1.4 to 1.8 times that at 20 °C.

2.3 Hydrological data collection

Bail-recharge tests were conducted at ten sites across the northern hemisphere cryosphere bridging a range of latitudes and climatic settings (Table 1; Figure 4). At Haut Glacier d'Arolla, Switzerland, and Fountain Glacier Bylot Island (HACH and FGBI, respectively), holes were drilled at strategic locations along transects or semi-randomised grids within a defined supraglacial micro-catchment, whilst on the K-Transect of western Greenland (GRDS), nine holes were distributed across a 30 × 30 m grid. At other sites including those in Sweden (SGSE, RGSE), Austria (RMOS, GBOS), at the Greenland Ice Sheet margin (GRKM) and Svalbard (PBSV, FFSV) experiments were conducted opportunistically using glacier-wide randomised grid sampling or short transects over smaller, hydrologically active areas.

At all sites, 36 cm deep auger-holes were drilled using a 5 cm diameter Kovacs drill. The auger-hole depth enabled the upper 30 cm of the weathering crust to be examined, since there is a 6 cm 'dead space' at the base of the piezometer. Auger-holes were emptied using a biOrb™ manual syphon with a 5 cm nozzle head. The piezometer was inserted immediately, and recharge monitored at 2 s intervals. In cases where auger-holes were reused during a single day, ablation resulted in some widening of the uppermost 5 cm of auger-hole, but this had negligible influence upon the bail-recharge experiments due to the water table typically found ~14 cm from the glacier surface. The representativeness of the 36 cm deep auger-holes is assessed in Section 3.1 below.

Time-series of auger-hole water column height were converted to recharge water volume and corrected to account for water displacement arising from piezometer installation. Recharge curves were manually examined and divided into three distinct stages (Figure 5): (i) Stage 1 is a linear stage

which represents pressure driven recharge as a result of the artificial water head generated by the presence of the bailed auger-hole within the weathering crust; (ii) Stage 2 is a non-linear decreasing stage (i.e., recharge rate falls with time/rise in auger-hole water level), identified as representing a reduction in the influence of pressure-driven flow from three dimensions, and representing the flow of water through an undisturbed weathering crust (i.e., the idealised water table in Figure 2). Stage 3 is a linear stage with a gradient of 0, at which point water in the auger-hole is equilibrated with the level of the water table in the surrounding weathering crust (Figure 5).

Hydraulic conductivity, *K*, was calculated using Equations 1 and 2, where recharge rate derived from Stage 2 defines *Q,* and the stable water level at Stage 3 substituted for *y*. To ensure y ≠ 0, the Stage 3 auger-hole recharge data was filtered and limited to 0.01 V below the voltage observed for the static equilibrium water table water depth. In the discrete cases where the auger-hole exhibited 'incomplete recharge', either *y* was defined using a repeat or proximal measurement within 10 minutes of the curtailed measurement, or a mean water table depth for the specific glacier was used.

In the absence of detailed weathering crust density profiles with depth, we parameterised D (Eq. 4) to be 40 cm which ensured the ratio L/R_w equalled 14.4; consequently, following Bouwer and Rice (1976)'s condition that for $7 < L/r_w < 16$, constants *A* and *B* (Equation 3) are defined as 2 and 0.25, respectively. The uncertainty related to this assumption was negligible: in cases where D exceeds 40 cm, there is no change in the estimated *K*, while if *D-h* was reduced to the smallest possible value within the piezometer's measurement capabilities, there is an underestimate in *K* of only 6.5%. To quantify the uncertainties that resulted from the manual definition of Stage 2 in the recharge curve, a subsample of 25 recharge curves were selected randomly, covering all glaciers and a representative range of recharge rates. By identifying potential errors in the location of the transition between Stages 1 and 2 in this subsample, uncertainty in the calculated *K* was estimated as ± 4.8%, and again considered negligible.

2.4 Ancillary data collection

Automated weather stations (AWSs) were installed locally at all sites apart from GBOS and RMOS. In a few cases missing data was interpolated using data from the nearest alternative weather station. Where SWR_{in} data was unavailable it was modelled (Irvine-Fynn *et al.*, 2014) and a cloud cover correction applied using observations from local weather stations (see Greuell *et al.*, 1997). Modelled data correlated well with measured values during the period for which directly measured SWR_{in} was available ($r^2 = 0.81$). Using these data, cumulative energy input (MJ m^{-2}) from SWR_{in} since the last freeze event (i.e. temperature < 0 °C) was calculated to explore the qualitative observations of Muller

and Keeler (1969) regarding weathering crust development processes. For glaciers with full meteorological data, meltwater production (M) was modelled using a point-based energy balance model (Brock and Arnold, 2000) at all auger-hole sites for each glacier, with a modification applied to arctic glaciers to account for the high solar azimuth (Irvine-Fynn *et al.*, 2014).

3. Results

3.1 Piezometer evaluation

Firstly, to assess the representativeness of the 36 cm auger-holes, comparisons were made with proximate holes with depths of 16 and 26 cm at FGBI and GRDS, with additional 46 cm deep auger holes at the former site (Figure 6). Auger-holes were located within ~0.5 m of each other over a visually similar ice type, to minimise the influence of hole-to-hole disturbance and mitigate spatial variations in ice structure. Shapiro-Wilk tests highlighted the hydraulic conductivity data were not normally distributed at either site. For FGBI, an independent samples median test highlighted no significant difference in median values of *K* between different hole depths ($p < 0.05$). However, a Kruskall-Wallis test indicated a difference in distribution of *K* values across the four contrasting auger-hole depth groups ($p < 0.05$), with the bounds of total ranges and interquartile ranges decreasing with an increase in auger-hole depth. Dunn's post-hoc testing indicated that only the 46 cm and 16 cm groups were significantly differently distributed from each other ($p < 0.05$). Similarly, for GRDS, an independent samples median test indicated that median *K* were significantly different between the three groups ($p < 0.05$). A Kruskall-Wallis test indicated that distribution of *K* across the three depth groups was significantly different ($p < 0.05$), with Dunn's post hoc testing indicating the presence of a pairwise significant difference in data distribution only between the 26 cm and 36 cm groups ($p < 0.05$). However, there is no significant difference between any of the depth groups and the overall median for GRDS.

As there is no systematic significant difference between medians for auger-holes of 16, 26, 36 and 46 cm in depth, any of these depths could have likely been selected as a methodological optimum. A shallow hole would require a smaller volume of water to fill, and would enable a greater frequency of measurements to be recorded in a fixed period and may increase clarity of temporal trends, especially over a diurnal timescale. However, when the water table is low, shallow holes may be unsuitable as they may be perched above the water table, resulting in an inability to assess hydraulic conductivity. Conversely, a deeper auger-hole (e.g. 46 cm) would be unlikely to have such an issue, but would take longer to fill reducing the frequency of *K* measurements. As such we recommend and adopted 36 cm

as an optimum auger-hole depth as a compromise to maximise the frequency of data collection for assessment of weathering crust hydraulic parameters.

To ascertain the repeatability of the bail-recharge method, rapid (< 15 minutes) repeat measurements were undertaken at four sites (PBSV, SGSE, GRKM and GRDS). All repeat measurements were recorded within a maximum 30 minute window to minimise any temporal variations in *K*. During these repeats, a constant equilibrium water table depth was assumed (range within ±5 % of the mean) to prevent undesirable influence of a falling water table due to aquifer drainage upon *K*. Relative standard deviation (n = 19) across the four sites was 40.9%. Of note, the contrast in medians reported for varied auger-hole depths also all fell within this error associated with repeatability. Whilst this may appear initially to represent a high level of uncertainty in our estimates of *K*, typical ranges of *K* in groundwater studies cover a range of thirteen magnitudes (Freeze and Cherry 1979) and quantification of *K* to within one order of magnitude is usually sufficiently precise for most analyses Younger (2009). Our calculated relative standard deviation falls within this acceptable range, and as such, we are confident that our single-measure method provided suitably reliable and precise estimates of *K* within the weathering crust.

3.2 Quantification of and controls upon *K*

A total of 280 successful recharge experiments were conducted on 10 northern hemisphere glacier ablation zones. Twenty-five 'unsuccessful' experiments were reported in which holes were not refilled to > 6 cm depth; these were typically associated with cloudy and/or rainy conditions, but had no clearly systematic cause, and occurred apparently randomly across all glacier sites. Mean *K* across the eight field sites was 0.185 ± 0.019 m d^{-1} (σ = 0.310 m d^{-1}, range = 0.003 – 3.519 m d^{-1}). Mean permeability was 0.384 ± 0.060 m^2 (with a range from 0.018 – 3.451 m d^{-1}). Neither hydraulic conductivity nor permeability data were normally distributed (Shapiro-Wilk, n = 280 and 111, respectively, $p < 0.05$). Ranges and medians of *K* at each glacier plotted with site latitude as a variable (Figure 7) highlighted a potential relationship between latitude and *K*: a statistically significant, weak positive correlation existed between the variables (Spearman's $r = 0.140$, $p < 0.05$, n = 280).

To interrogate the environmental factors that may define *K*, specifically examining differing stages of weathering crust development, further non-parametric correlations were undertaken between *K* and potential explanatory variables. Such variables included water table height, as measured from the base of the 36 cm auger-holes according to the Stage 3 piezometer recharge records. The potential for the water table to be influenced by the melt rate and ingress of surface water into the weathering crust was further considered by using site altitude and the energy balance model melt output (M) for the 1-hour time period preceding the observation of *K* as explanatory variables. Further, based on

Muller and Keeler's (1969) conceptual model of weathering crust development, cumulative SWR_{in} receipt since (i) freezing, (ii) the previous rainfall event, and (iii) the period of dominant turbulent fluxes were calculated as variables.

Freezing of interstitial meltwater is may reduce interstitial pore size and decrease the hydraulic conductivity of the weathering crust. However, given the latent heat released during the refreezing of interstitial meltwater (see Paterson, 1994), a period of freezing air temperature for hours or even days is unlikely to result in complete re-freezing of the liquid component of the weathering crust. However, it is important to note that such a cold wave propagates downwards (Paterson, 1994; Irvine-Fynn *et al*., 2011a) so any refreezing will occur in the less dense, more porous upper weathering crust and hence may have a greater influence on *K* than would be expected. Rainfall events and cloudy periods, where turbulent fluxes dominate the energy balance equation (see Hock, 2005) are identified as crucial for "resetting" of the weathering crust surface (Muller and Keeler, 1969). Observations of summer rainfall are limited within our dataset, however we assume that precipitation, as measured at local AWSs, is in the form of rain either supported by *in situ* observations or as defined by air temperatures in excess of 4 °C. For the available data, two periods of rainfall were identified, one at HACH, comprising a 10 hour period of overnight rainfall (17 mm total) and another at SGSE/RGSE, where 2.4 mm of rain fell in eight hours. Melt modelling data are used to determine the ratio of SWR_{in}:turbulent fluxes at each glacier site, with a period of dominant turbulent energy flux (DTEF) defined as when > 50 % of energy for melt is supplied by turbulent fluxes for a duration of at least three hours. This duration is selected to ensure that the predominant weather pattern is that of a cloudy sky, rather than a low sun angle and high air temperatures which can occur during sunrise and sunset. Available meteorological data allowed for determination of this variable at GRDS, & SGSE/RGSE. For GRDS, two DTEF periods were observed, both between midnight (00:00) and 07:00 when the solar azimuth was low: total melt during the two periods was 1.71 and 0.57 mm water equivalent (w.e.). A more marked period of DTEF was observed at RGSE and SGSE, with a 37 and 39 hour DTEF period with 27.06 and 25.03 mm w.e. of melt respectively. With freezing, rainfall and DTEF periods being indicative of (at least partial) resetting of the weathering crust, cumulative SWR_{in} should identify the subsequent increase in near-surface ablation, the disaggregation of ice crystals and increasing porosity and hydraulic conductivity.

The following significant ($p < 0.01$) monotonic correlations are highlighted between *K* and the following independent variables (Table 2): a) negative correlation with cumulative SWR_{in} since freezing; b) strong negative correlation with cumulative SWR_{in} since previous DTEF period; iii) weakly negative correlation with altitude, c) strongly positive correlation with water table height.

Similar analysis was undertaken for permeability (κ; Table 3) for PBSV and HACH located at each extreme of the latitudinal range of field sites within this study. Mean auger-hole water temperatures of 0.57 ± 0.02 °C and 0.17 ± 0.01 °C, and ranges of 0.20 – 0.90 and 0.10 – 0.40 °C, respectively. This yielded permeability values ranging over 3 orders of magnitude from 0.018 and 3.45 m^2. However, with auger-hole water temperature data only available for two glaciers, our interpretations are limited. By estimating a mean water temperature for all other glaciers, any correlations with environmental variables would simple mirror those reported for *K* (see Eq. 5).

4. Discussion

Ablating glacier surfaces are characterised by a porous ice weathering crust which may influence meltwater, sediment, microbial cell and nutrient storage and transport (Hodson et al., 2007; Munro, 2011; Irvine-Fynn et al, 2012; Edwards et al., 2011; Stibal et al., 2012). Here, we have presented data from a low-cost capacitance piezometer which, to our knowledge, is the first comprehensive set of measurements across multiple glacier sites using a standardised methodology to describe *K* for weathering crust ice.

4.1 Application of piezometer and Darcian flow model to the weathering crust

The piezometer described provides high-resolution water level data. The application of the piezometer in supraglacial environments enabled quantification of the hydraulic properties of the weathering crust and was used to test the applicability of Darcy's Law to the weathering crust. Darcy's Law describes diffuse water flow through a homogenous porous media and is not applicable where flow is confined to or influenced by discrete conduits ('karstic flow': Moore, 2002). Karstic flow would cause the recharge curves to show irregular or abrupt step-changes where water suddenly enters a conduit (e.g. Hartmann*, et al.*, 2014). This characteristic or phenomenon in the recharge curves was not observed in our data, indicating that flow through the weathering crust appears to be effectively homogenous at the synoptic scale and that Darcy's Law can be applied broadly with confidence to weathering crust hydrology.

4.2 Hydraulic conductivity of the weathering crust

At the ten sites examined across the northern hemisphere, mean weathering crust *K* was 0.185 ± 0.019 m d^{-1}. This value is equivalent to those reported for sandstone (10^{-1} – 10^{1} m d^{-1}), or stratified clay soil (10^{-1} – 10^{2} m d^{-1}) (Bear, 1972) and hence, hydrologically, the glacial weathering crust can be considered as a poor, impervious aquifer. This also compares well, albeit an order of magnitude lower, to the recent 10^{0} – 10^{2} m d^{-1} estimates for the hydraulic conductivity of firn on alpine glaciers (e.g. Fountain

1989; Schneider, 1999) and the Greenland Ice Sheet (e.g. Miller *et al*., 2017). Our *K* values are the same order of magnitude as those reported for ablating glacier ice by Cook *et al.* (2016a), and similar to the lower-order estimates given by previous site-specific studies (e.g. Karlstrom*, et al.* 2014; Larson, 1977; Theakstone and Knudsen, 1981; Wakahama, 1978; Wakahama*, et al.*, 1973). Our estimated ranges of weathering crust hydraulic conductivity still encompassed the values derived from Medenhall and Llewellyn Glaciers (Juneau Icefield, Alaska/British Columbia) despite the absence of such a maritime environment in the study sites reported here.

The estimates of *K* in the weathering crust approaching that of sandstone or clay would see surprising given the degrading near-surface ice surface would suggest a higher porosity and potentially an increased hydraulic conductivity. However, hydraulic permeability and conductivity are also governed by the scale of and linkage between void spaces in a porous medium (Bear, 1972). Both the angularity of ice crystals and the immobile viscous water layers that surround them (Nye, 1991) reduce the hydraulic conductivity through, respectively, increasing micro-scale flowpath tortuosity and reducing permeability. Water movement in the uppermost 2 m of a glacier is typically driven upward due to the near-surface water pressure gradient (Llibourty, 1996) that can be influenced by meteorological conditions and is complicated further by the capillary force that retains and restricts water flow (Bear, 1972), allowing flow in opposition to the gravity- and slope-driven directions. Moreover, observations of local water tables identified in open cryoconite holes suggests that the water table is commonly several centimetres to three decimetres below the ice surface (Cook *et al*., 2016a,b), and so *K* is retrieved for depths below the most porous surface ice. Combined with the near-surface density gradient, these mechanical conditions may in part explain the low *K* identified for the apparently porous weathering crust.Studies conducted in the 1970s and 1980s used contrasting methods, including dyes such as ink (Wakahama*, et al.*, 1973) and fluorescein (Theakstone and Knudsen, 1981). Ink and tracer dyes such as fluorescein and rhodamine are highly dispersive within water (Smart and Laidlaw, 1977); therefore, the use of dyes may result in an overestimation of *K,* as the tracer will likely have dispersed through the sub-surface water column rather than acting conservatively and matching the water flow rate. Theakstone and Knudsen's (1981) work focused on the quantification of meltwater flow rates through the supraglacial drainage network, and they only estimated the delay to flow caused by the weathering crust as a component of this. Despite this difference in emphasis, our upper estimates for *K* coincide with Theakstone and Knudsen's median estimates, while difference compared to the *K* value reported for Medenhall Glacier (Karlstrom *et al*., 2014) may simply be due to the particular environmental and climatic setting, solar radiation receipt and synoptic progress through individual melt seasons.

One issue arising with the use of pumped wells (e.g. Larson, 1977) for the estimation of *K* in glaciological environments is that the technique requires the addition of water, which causes a local increase in water table height. As SWR_{in} receipt decreases with depth in the near-surface (Cook *et al.*, 2016a) it is expected that pore size, permeability and *K* will also decrease. The inverse is also true, so by introducing a false rise in the water table, *K* is measured through more porous ice which is typically above the equilibrium water table and hence not necessarily describing *K* for the true transmission of meltwater at a given point in time, and generating artificially elevated estimates of its value. To emphasise this assertion, our data show that an increase in water table height correlates with an increase in *K* and highlight the need to consider methods of describing hydraulic conductivity cautiously.

4.3 Controls upon hydraulic conductivity of the weathering crust

In the weathering crust, the mechanism for pore enlargement is hypothesised as the cumulative receipt of subsurface SWR_{in} and internal melt of ice (Cook *et al.*, 2016a; Hoffman *et al.*, 2014; Müller and Keeler, 1969). This is evidenced by the lower bulk density and greater intergranular pore space of the weathering crust when contrasted with un-weathered glacier ice (LaChapelle, 1959, Nye, 1991). This enlargement of inter-crystalline pores would result in an increase in hydraulic conductivities. The energy available for weathering crust development is constrained by latitude, typically with more intense SW_{in} and higher summer season air temperature even at elevation in lower latitudes. Latitude is weakly positively correlated with *K*, but Figure 7 indicates that the highest *K* values are observed in the 67 – 72 °N latitude band. This relationship is complicated by regional climatology, synoptic meteorology and local altitude and topography (Barry, 2013). For example, summer cloud cover and precipitation are common in both the Alps (e.g. Rudolph *et al*., 2011) and High-Arctic Svalbard (e.g. Førland and Hanssen-Bauer, 2000), and these conditions are known to reduce or minimise weathering crust development (Muller and Keeler, 1969). Shading by surrounding terrain will also affect SWR_{in} receipt and moderate the formation and evolution of a porous surface ice layer, while particularly in mid- and high-latitudes, as a consequence of solar geometry, glacier orientation and surface slope may become more influential. While sites characterised by higher katabatic wind speeds may experience elevated turbulent energy fluxes that reduce the efficacy of weathering crust development.

The analyses seeking to identify such additional potential controlling factors on *K* in terms of cumulative SWR_{in} receipt since any partial or complete 'resetting' of the weathering crust resulted in less intuitive conclusions. The negative correlations between *K* and SWR_{in} since last freezing and DTEF periods indicated that as the weathering crust developed, there was a reduction in the hydraulic

permeability. This was unexpected as low radiative and high turbulent energy transfers, such as cloudy periods, often including rainfall, have been anecdotally linked with weathering crust removal (Müller and Keeler, 1969). Consequently, such synoptic conditions were expected to be associated with lowered *K*, as was evident from several of the 'failed' recharge experiments. Here, to explain the apparently inverse relationship between *K* and cumulative SWR_{in}, we suggest that the development and rise of a water table is not necessarily coincidental with progressive ice crystal disaggregation; the rise in the water table may lag behind the creation of intergranular void space implying a low water table is associated with low *K* values. Supporting this argument is the observation that *K* is not correlated solely with the melt that might be expected to increase the water table height and hence hydraulic conductivity. This implies that additional processes are occurring, which preclude any direct relationship between melt rate and *K*: for example, there could be refreezing at depth within the weathering crust and reduction of liquid water volume, or the low transmission rates incur delay as pore spaces are filled. Here, there may be analogies with the progress of the wetting front in a snowpack (e.g. Marsh and Woo, 1984) or infiltration to frozen soil (e.g. Gray *et al*., 2001), but to develop this level of process understanding would require further investigation.

The additional complexity hydrology itself may impart on defining *K* is best evidenced by the positive relationship between *K* and water table height. Observations from cryoconite holes suggests there is a variable water table height within the weathering crust both at sub-diurnal and synoptic time-scales (e.g. Cook *et al.*, 2016a). These variations may arise from the bulk density increase with depth within the weathering crust, or because of a changing local base-level. Once the ability of the weathering crust to transport water is exceeded by the melt input the water table will rise into the increasingly more porous near-surface ice, and the piezometer derived *K* value increases. Hydraulic conductivity may, in this scenario, also rise if the base-level for the drainage pathway remains broadly the same due to the dampened response of the supraglacial stream network to peak melt (e.g. Munro, 2011; Smith *et al.*, 2015, 2017) and the hydraulic gradient increases. However, as the weathering crust is drained as melt rates and associated water inputs reduce overnight, and the supraglacial stream base level drops, the water table and pressure head falls, hence *K* is reduced. Our feedback loop between meltwater input, water table height and *K* would explain why *K* and melt do not directly correlate as a response time is required, dependant on infiltration rate, for the water table level to rise.

Our data from 10 glacier sites shows that *K* exhibited values over a range of four magnitudes (relative standard deviation of ~180%) and even upon individual glaciers there is a high local-scale variability (Figure 7). While the relationships described above provide some indications of conceivable causes in the variability in *K* values, there are clearly complex interactions between potential driving meteorological variables, which are problematic to disentangle without further study. However, one

further aspect which influences the fabric of the weathering crust and hence the nature of the pores within is the microscale ice-structure, which is difficult to characterise and quantify and is not included within this dataset. Ice structure and fabric will directly condition pore size and shape, interstitial connectedness and tortuosity, and therefore likely influence the hydraulic behaviour of the weathering crust. Ice structure and fabric can vary across a range of length scales (see Hambrey and Lawson, 2000; Hudleston 2015). Consequently, crystal size, packing and orientation may play an important role in defining the rate and location at which water infiltrates and is transferred through the weathering crust, by controlling potential pore size, shape and geometry once crystal boundaries are preferentially melted to form pores.

Our data highlight the hydrological properties of the weathering crust are influenced and conditioned by an array of influential factors, ranging from the meteorological conditions and their synoptic progression prior to evaluation of *K* and to the hydrological and structural characteristics of the near-surface ice itself. We also hypothesise that glacier ice dynamics and net ablation may have the capacity to modulate the weathering crust and its hydrological behaviour: glaciers exhibiting higher ice emergence rates may offset the evolution of a deeper porous surface layer, and enhanced rates of ablation and runoff may lead to an abundance of rills and streams which through energy transfers and evolving topographic variability can degrade the weathering crust and slow its vertical evolution and spatial extent. Such hydrological disturbance may also be affected by glacier surface slope (e.g., Hodson *et al*., 2007; Mantelli *et al*., 2015; Rippin *et al*., 2016). Here, it is clear that that more systematic surveys of *K* under constrained environmental parameters, and over extended time-frames, are required to better define the primary drivers and rates of weathering crust development and its spatial and vertical extent at (sub) catchment to glacier scales.

4.4 Hydrological role of the weathering crust and relevance to impurity transport

This study highlights a typically overlooked component of the supraglacial hydrological system. Near-surface glacier ice has traditionally been considered as essentially impermeable (e.g. Hodgkins, 1997) with an abrupt, almost immediate hydrological response time (e.g. Fountain and Walder, 1998). Our data emphasises the weathering crust as a hitherto neglected yet important aspect of supraglacial hydrology. The presence of a water table at depth below the ice surface emphasises the potential for short-term meltwater storage, retention and delay in runoff. We propose that as surface ice ablates during the ablation season, under clear sky conditions, the weathering crust develops (Muller and Keeler, 1969) and meltwater is routed through this near-surface layer. As our data show, meltwater flow through the weathering crust can be relatively slow, yet supraglacial stream discharge response to peak melt typically occurs within < 12 hours (Munro, 2011). The hydraulic conductivities calculated

here, coupled with typical ≤ 10^1 m channel spacing upon glacier surfaces (e.g. Karlstrom *et al.*, 2014), imply that a parcel of meltwater could remain within the weathering crust for a minimum of 34 hours. Therefore, our observations directly support the notions of hydrological delay and water storage within the weathering crust conjectured by Munro (2011) and Smith *et al*. (2017).

At synoptic and diurnal time-scales, we hypothesise that in response to the energy balance, additional 'new' meltwater enters the weathering crust causing the water table to rise, which positively influences *K*, and either overrides or displaces 'old' stored or retained meltwater. This type of water turnover is common for rainfall events in terrestrial environments (e.g. Brutsaert, 2005; Lu and Godt, 2013). When melt production exceeds the infiltration rate of the weathering crust, or the water table rises to the surface, it would be expected that saturated sheet flow might occur over the surface; however, due to the complex nature of glacier surfaces, sheet flow is uncommon and was not observed during our observation periods, and drainage via rills and small streams evolves quickly (e.g. Mantelli *et al*., 2015). However, the observation of *K* being dependent on water table elevation suggests the hydraulic properties exhibit a gradient with depth in the near-surface which is also spatially and temporally variable. The proportions of meltwater that may be delayed at a variety of time-scales in their delivery to supraglacial rill and stream networks and the subsequent modulation of channel hydrographs remain undefined.

The presence of a near-surface aquifer on ablating glacier surfaces with a low hydraulic conductivity may also have significant implications for the transfer of impurities across exposed ice and affect biogeochemical cycling. Here, we argue that based on contemporary understanding there is a need for future research to explore a range of these potential affects. Considering the characteristic and ubiquitous presence of fine inorganic dust (e.g. Takeuchi, 2002; Oerlemans *et al*., 2009), microbes (e.g. Hodson *et al*., 2008; Stibal *et al*., 2012; Edwards and Irvine-Fynn, 2014) and other particulate impurities and contaminants (e.g. Hodson, 2014) on glacier surfaces, the poor hydraulic conductivity of the weathering crust may have important implications on the transport rate of such particulates. To date, there has been no clear or detailed assessment of the rates at which impurities are transferred over ablating ice surfaces. Irvine-Fynn *et al.* (2012) reported inefficient transport processes through, and storage of microbial cells within the near-surface of an Arctic glaciers. Here, the low *K* values reported for numerous glaciers align well with such an assertion of inefficient water transfer. However, the relationship between impurity transport and *K* is unlikely to be a simple linear function due to the potential of the weathering crust to act as mechanical filter, preventing transfer of particles with diameters in excess of pore sizes, or bio- and physio-chemical processes resisting or accentuating impurity transport (e.g. Mader *et al*., 2006; Jepsen *et al*., 2006, 2010; Dolev *et al*., 2017). Therefore, fluctuations in the water table and of varied hydraulic conductivity at diurnal or synoptic time-scales,

or over space, may be crucial in defining the character of impurities transported through or from a glacier's surface. Indeed, recent work has suggested that water flux and the hydraulic delivery of dissolved nutrients within meltwater to surface microbial habitats may be a crucial influence for microbial community structure and activity (e.g. Edwards *et al*., 2011; Dubnick *et al*., 2017), and controls downstream ecology and characteristics (e.g. Singer et al., 2012; Wilhelm *et al*., 2013). Furthermore, when combined with typical *in situ* doubling times of the water-borne cryospheric microbial communities of < 60 days, and in some instances < 5 days (Anesio *et al.*, 2010), and clear evidence of their capacity to influence nutrient cycling (Scott *et al*., 2010), the potential for the supraglacial weathering crust as a microbial habitat (Irvine-Fynn and Edwards, 2014) merits further investigation. Specifically, the retention of mineral dust and microbes within the weathering crust holds the potential to contribute to supraglacial biogeochemical cycles. For example, increased residence time within the weathering crust permits greater interactions between dust, dilute nutrients, low-density bacterial hosts and their viral parasites (Rassner et al 2016). The hydraulics of the weathering crust, and the recognition of 'old' and 'new' meltwaters, may hold potential influence on the transfer rates for solutes and dissolved organic compounds or contaminants within the glacier system. However, the *in situ* fate of supraglacial solutes, organic compounds and contaminants during the ablation season still remains poorly characterised.

As both Grannas *et al*. (2013) and Hotaling *et al*. (2017) concluded, there remains a pressing need to better constrain the nature and variability of supraglacial hydrological flowpaths particularly to define their impact on contaminant and impurity transfer, microbial communities and biogeochemical function both for glacier surfaces and glacier-fed ecosystems. This is particularly significant under the spectre of projected future changes to glacier and ice sheet runoff regimes (e.g. Franco *et al*., 2013; Bliss *et al*., 2014). In many glacierised regions, atmospheric warming, rising snowlines and expanding ablation areas may result in extensive supraglacial hydrology even as total glacier areas decline. Similarly, glacier thinning and cooling in higher latitudes (e.g. Irvine-Fynn *et al*., 2011a; Delcourt *et al*., 2013) may also promote an increasing dominance of supraglacial hydrology. Consequently, understanding the influence that the weathering crust has on modulating supraglacial runoff and its characteristics is important to improve predictive hydrological models. This assessment of weathering crust hydrology presents a first step to better characterising this commonly overlooked supraglacial flowpath, and exploring the controls that dictate spatial and temporal variation in hydraulic conductivity of near-surface glacier ice.

5. Conclusions

We present a robust but simple piezometer probe design that permits low-cost, high-resolution, repeatable water level monitoring. The economical nature of the piezometer design, combined with its limited power requirements, make it ideally suited to spatially widespread deployment in remote locations and for hydrological applications beyond those described here. We describe a field methodology that allows spatially widespread monitoring of glacier weathering crust water level fluctuations at multiple sites. Data collected from a spatially extensive suite of field sites allows examination of weathering crust *K*, and we quantify a mean *K* of 0.185 m d^{-1} which is an equivalent value to that seen for sandstone and firn and, therefore, leads us to regard the weathering crust as a hydrologically poor, impervious aquifer that can delay water transfer through the supraglacial hydrological system and acting as a transient, multi-day storage reservoir within this network. Our data show unequivocal evidence for spatially and temporally varying supraglacial storage and regulation of meltwater hypothesised by Munro (2011) and Smith *et al*. (2017). This role of the weathering crust as a regulator of meltwater egress has the potential to impact not only on meltwater discharge but also the supraglacial ecosystem, through influencing the transport and residence time of microbes, fine mineral grains, contaminants and associated nutrients. Such impurity and biogeochemical fluxes, and their basin-scale export, have consequent impacts upon the supraglacial and down-stream environments at a range of spatial and temporal scales. Our analysis demonstrates that the precise nature of the controls that drive the hydrological characteristics of the weathering crust are clearly complex and multi-faceted. Although water table height clearly exerts a fundamental control on apparent hydraulic conductivity, detailed investigation of the evolution of the weathering crust, and the role of hyper-local ice structure and crystallography and consequent impacts on near-surface sedimentary- and eco- systems likely represents a fruitful avenue for further investigation.

Acknowledgements

Financial support for this work was gratefully received from: Aberystwyth University (Department of Geography and Earth Sciences), Gilchrist Educational Trust, EU F7 INTERACT (grant: SCARFACE to TDI and AE), Royal Geographical Society (fieldwork grant: to ITS), Royal Society (grant: RG130314 to AE and TDI), Scottish Arctic Club (grant: to ITS), PSCP and NSERC (for support on Bylot Island: to BJM), and the Climate Change Consortium for Wales (C3W grant: Proof of Concept to TDI). JMC acknowledges the Rolex Awards for Enterprise. TDI and JMC also acknowledge NERC Consortium Grant 'Black and Bloom' (NE/M021025/1). The Dark Snow Project, and Karen Cameron and Jason Box, are thanked for the support in Greenland. The authors wish to thank Stephen Jennings, Ottavia Cavalli, Stephen

Brough, Sarah St Germain, Michael Hambrey and Jayne Kamintizis for invaluable assistance throughout various field campaigns. Andy Porter provided generous guidance with regards to the electronics and drawing the circuit diagrams in Figure 2. Dave Kelly (Aberystwyth) is thanked for refinement and construction of the piezometer probes, developing prototypes built by Stephen Norburn (Sheffield). Jon Bridge and two anonymous reviewers are thanked for insightful comments that improved earlier versions of the manuscript.

Reference List

Abermann J, Lambrecht A, Fischer A, Kuhn M. 2009. Quantifying changes and trends in glacier area and volume in the Austrian Ötztal Alps (1969-1997-2006). The Cryosphere **3**: 205-215. DOI: 10.5194/tc-3-205-2009

Adhikary S, Nakawo M, Seko K, Shakya, B. 2000. Dust influence on the melting process of glacier ice: experimental results from Lirung Glacier, Nepal Himalayas. IAHS Publication **264**: 43-52.

Amoozegar A, Warrick AW. 1986. Hydraulic conductivity of saturated soils: field methods. In Methods of soil analysis part I: physical and mineralogical methods, Klute A (ed). Soil Science Society of America: Wisconsin, USA; 735-770.

Anesio AM, Sattler B, Foreman C, Telling J, Hodson A, Tranter M, Psenner R. 2010. Carbon fluxes through bacterial communities on glacier surfaces. Annals of Glaciology **51**: 32-40. DOI: 10.3189/172756411795932092

Barry RG. 1992. Mountain weather and climate (2nd ed.). Routledge: London.

Baxter LK. 1997. Capacitive Sensors: Design and Applications, IEEE Press, New York.

Bear J. 1972. Dynamics of fluids in porous media. Elsevier: London

Bettinetti R, Quadroni S, Boggio E, Galassi S. 2016. Recent DDT and PCB contamination in the sediment and biota of the Como Bay (Lake Como, Italy). Science of the Total Environment **542A**: 404-410. DOI: http://dx.doi.org/10.1016/j.scitotenv.2015.10.099

Bizzotto EC, Villa S, Vaj C, Vighi M., 2009. Comparison of glacial and non-glacial-fed streams to evaluate the loading of persistent organic pollutants through seasonal snow/ice melt. Chemosphere, **74**(7): 924-930. DOI: 10.1016/j.chemosphere.2008.10.013

Björnsson H. 1981. Radio-Echo Sounding Maps of Storglaciaren, Isfallsglaciaren and Rabots Glaciar, Northern Sweden. Geografiska Annaler **63A**: 225-231. DOI: 10.2307/520835

Bliss A, Hock R, Radic V. 2014. Global response of glacier runoff to twenty-first century climate change. Journal of Geophysical Resarch: Earth Surface **119**(4):717-730. DOI: 10.1002/2013JF002931

Bogdal C, Scheringer M, Schmid P, Bläuenstein M, Kohler M, Hungerbühler K. 2010. Levels, fluxes and time trends of persistent organic pollutants in Lake Thun, Switzerland: Combining trace analysis and multimedia modeling. Science of the Total Environment **408**: 3654-3663. DOI: http://dx.doi.org/10.1016/j.scitotenv.2010.04.038

Bogdal C, Schmid P, Zennegg M, Anselmetti FS, Scheringer M, Hungerbühler K. 2009. Blast from the Past: Melting Glaciers as a Relevant Source for Persistent Organic Pollutants. Environmental Science & Technology **43**: 8173-8177. DOI: 10.1021/es901628x

Bouwer H, Rice RC. 1976. A slug test determining hydraulic conductivity of unconfined aquifers with completely or partially penetrating wells. Water Resources Research **12**: 423-428

Brandt RE, Warren SG. 1993. Solar-heating rates and temperature profiles in Antarctic snow and ice. Journal of Glaciology **39**: 99-110

Brock BW, Arnold NS. 2000. A spreadsheet-based (Microsoft Excel) point surface energy-balance model for glacier and snow melt studies. Earth Surface Processes and Landforms **25**: 649-658

Brock BW, Willis IC, Sharp MJ. 2000. Measurement and parameterization of albedo variations at Haut Glacier d'Arolla, Switzerland. Journal of Glaciology **46**: 675-688. DOI: 10.3189/172756500781832675

Brugger KA. 2007. The non-synchronous response of Rabots Glaciär and Storglaciären, northern Sweden, to recent climate change: a comparative study. Annals of Glaciology **46**: 275-282. DOI: 10.3189/172756407782871369

Brugger KA, Refsnider KA, Whitehill MF. 2005. Variation in glacier length and ice volume of Rabots Glaciär, Sweden, in response to climate change, 1910 - 2003. Annals of Glaciology **42**: 180-188. DOI: 10.3189/172756405781813014

Brutsaert W. 2005. Hydrology: an introduction. Cambridge University Press

Conway H, Gades A, Raymond CF. 1996. Albedo of dirty snow during conditions of melt. Water Resources Research **32**: 1713-1718. DOI: 10.1029/96WR00712

Cook JM, Hodson AJ, Irvine-Fynn TDL. 2016a. Supraglacial weathering crust dynamics inferred from cryoconite hole hydrology. Hydrological Processes **30** (1): 433-446. DOI: 10.1002/hyp.10602

Cook J, Edwards A, Takeuchi N, Irvine-Fynn T. 2016b. Cryoconite: the dark biological secret of the cryosphere. Progress in Physical Geography, **40**(1): 66-111.

Cutler PM, Munro DS. 1996. Visible and near-infrared reflectivity during the ablation period on Peyto Glacier, Alberta, Canada. *Journal of Glaciology* **42**: 333-340

Delcourt C, van Liefferinge, Nola M, Pattyn, F. 2013. The climate memory of an Arctic polythermal glacier. Journal of Glaciology **59**(218): 1084-1092. DOI: 10.3189/2013JoG12J109

Derikx L. 1973. Glacier discharge simulation by groundwater analogue. IAHS Publication **95**: 29-40.

Dolev MB, Bernheim R, Davies PL, Braslavsky I. 2017. Putting life on ice: bacteria that bind to frozen water. Journal of the Royal Society Interface **13**: 20160210. DOI: 10.1098/rsif.2016.0210

Dubnick A, Kazemi S, Sharp M, Wadham J, Hawkings J, Beaton A, Lanoil B., 2017. Hydrological controls on glacially exported microbial assemblages. Journal of Geophysical Research: Biogeosciences, **122**(5): 1049-1061. DOI: 10.1002/2016JG003685

Edwards A, Anesio AM, Rassner SM, Sattler B, Hubbard B, Perkins WT, Young M, Griffith GW. 2011. Possible interactions between bacterial diversity, microbial activity and supraglacial hydrology of cryoconite holes in Svalbard. ISME J **5**: 150-160. DOI: 10.1038/ismej.2010.100

Edwards A, Pachebat JA, Swain M, Hegarty M, Hodson AJ, Irvine-Fynn TDL, Rassner SME, Sattler B. 2013. A metagenomic snapshot of taxonomic and functional diversity in an alpine glacier cryoconite ecosystem. Environmental Research Letters **8**: 035003. DOI: 10.1088/1748-9326/8/3/035003

Fischer A. 2010. Klima und Gletscher in Obergurgl. In Glaziale und periglaziale Lebensräume im Raum Obergurgl, Koch E-M, Erschblamer B (eds). Innsbruck University Press: Innsbruck; 53.

Førland EJ, Hanssen-Bauer I. 2000. Increased precipitation in the Norwegian Arctic: true or false? Climatic Change, **46**, 485-509.

Fountain AG. 1989. The storage of water in, and hydraulic characteristics of, the firn of South Cascade Glacier, Washington State, USA. Annals of Glaciology, **13**: 69-75.

Fountain AG, Walder JS. 1998. Water flow through temperate glaciers. Reviews of Geophysics **36**: 299-328

Freeze RA, Cherry JA. 1979. Groundwater, Prentice-Hall, pp.604.

Franco B, Fettweis X, Erpicum M. 2013. Future projections of the Greenland ice sheet energy balance driving the surface melt. The Cryosphere **7**: 1-18. DOI:10.5194/tc-7-1-2013

Gleason CJ, Smith LC, Chu VW, Legleiter CJ, Pitcher LH, Overstreet BT, Rennermalm AK, Forster RR, Yang K. 2016. Characterizing supraglacial meltwater channel hydraulics on the Greenland Ice Sheet from in situ observations. Earth Surface Processes and Landforms **41**(14): 2111-2122.

Grannas A, Bogdal C, Hageman K, Halsall C, Harner T, Hung H, Kallenborn R, Klán P, Klánová J, Macdonald R. 2013. The role of the global cryosphere in the fate of organic contaminants. Atmospheric Chemistry and Physics **13**: 3271-3305

Gray DM, Toth B, Zhao L, Pomeroy JW, Granger RJ. 2001. Estimating areal snowmelt infiltration into frozen soils. Hydrological Processes, **15**(16): 3095-3111.

Greuell W, Knap WH, Smeets PC. 1997. Elevational changes in meteorological variables along a midlatitude glacier during summer. Journal of Geophysical Research: Atmospheres **102**: 25941-25954. DOI: 10.1029/97JD02083

Hagen JO, Liestøl O, Roland E, Jørgensen T. 1993. Glacier Atlas of Svalbard and Jan Mayen. Norsk Polarinstitutt: Oslo

Hambrey, M.J. and Lawson, W., 2000. Structural styles and deformation fields in glaciers: a review. Geological Society, London, Special Publications, **176**(1):59-83.

Hartmann A, Goldscheider N, Wagener T, Lange J, Weiler M. 2014. Karst water resources in a changing world: Review of hydrological modeling approaches. Reviews of Geophysics **52**: 218-242. DOI: 10.1002/2013RG000443

Hock R, Holmgren B. 2005. A distributed surface energy-balance model for complex topography and its application to Storglaciären, Sweden. Journal of Glaciology **51**: 25-36. DOI: 10.3189/172756505781829566

Hock R, Jansson P, Braun LN. 2005. Modelling the Response of Mountain Glacier Discharge to Climate Warming. In Global Change and Mountain Regions: An Overview of Current Knowledge, Huber UM, Bugmann HKM, Reasoner MA (eds). Springer Netherlands: Dordrecht; 243-252.

Hodgkins R. 1997. Glacier hydrology in Svalbard, Norwegian high arctic. Quaternary Science Reviews **16**: 957-973. DOI: http://dx.doi.org/10.1016/S0277-3791(97)00032-2

Hodson AJ. 2014. Understanding the dynamics of black carbon and associated contaminants in glacial systems. Wiley Interdisciplinary Reviews: Water **1**: 141-149. DOI: 10.1002/wat2.1016

Hodson AJ, Anesio AM, Ng F, Watson R, Quirk J, Irvine-Fynn TDL, Dye A, Clark C, McCloy P, Kohler J, Sattler B. 2007. A glacier respires: Quantifying the distribution and respiration CO2 flux of cryoconite across an entire Arctic supraglacial ecosystem. Journal of Geophysical Research **112**. DOI: 10.1029/2007jg000452.

Hodson A, Anesio AM, Tranter M, Fountain A, Osborn M, Priscu J, Laybourn-Parry J, Sattler B. 2008. Glacial ecosystems. Ecological Monographs, **78**(1): 41-67.

Hoffman MJ, Fountain AG, Liston GE. 2014. Near-surface internal melting: a substantial mass loss on Antarctic Dry Valley glaciers. *Journal of Glaciology* **60**: 361-374. DOI: 10.3189/2014JoG13J095

Holmlund P, Eriksson M. 1989. The Cold Surface Layer on Storglaciaren. *Geografiska Annaler*, **71A**: 241-244. DOI: 10.2307/521394

Hotaling S, Hood E, Hamilton TL. 2017. Microbial ecology of mountain glacier ecosystems: Biodiversity, ecological connections, and implications of a warming climate. *Environmental Microbiology*. vv, xxx-xxx.

Hudleston PJ. 2015. Structures and fabrics in glacial ice: a review. Journal of Structural Geology, **81**: 1-27.

Irvine-Fynn TDL. 2008. Modelling runoff form the maritime Arctic cryosphere: Water storage and routing and Midtre Lovenbreen. In Department of Geography. University of Sheffield; 359pp.

Irvine-Fynn TDL, Edwards A. 2014. A frozen asset: the potential of flow cytometry in constraining the glacial biome. Cytometry A **85**: 3-7. DOI: 10.1002/cyto.a.22411

Irvine-Fynn, T.D., Bridge, J.W. and Hodson, A.J., 2011b. In situ quantification of supraglacial cryoconite morphodynamics using time-lapse imaging: an example from Svalbard. Journal of Glaciology, **57**(204), pp.651-657.

Irvine-Fynn TDL, Edwards A, Newton S, Langford H, Rassner SM, Telling J, Anesio AM, Hodson AJ. 2012. Microbial cell budgets of an Arctic glacier surface quantified using flow cytometry. Environmental Microbiology **14**: 2998-3012. DOI: 10.1111/j.1462-2920.2012.02876.x

Irvine-Fynn TDL, Hanna E, Barrand NE, Porter PR, Kohler J, Hodson AJ. 2014. Examination of a physically based, high-resolution, distributed Arctic temperature-index melt model, on Midtre Lovenbreen, Svalbard. Hydrological Processes **28**: 134-149. DOI: Doi 10.1002/Hyp.9526

Irvine-Fynn TDL, Hodson AJ, Moorman BJ, Vatne G, Hubbard AL. 2011a. Polythermal Glacier Hydrology: A Review. Reviews of Geophysics **49**(4): RG00350. DOI: 10.1029/2010rg000350

Irvine-Fynn TDL, Moorman BJ, Williams JLM, Walter FSA. 2006. Seasonal changes in ground-penetrating radar signature observed at a polythermal glacier, Bylot Island, Canada. Earth Surface Processes and Landforms **31**: 892-909. DOI: 10.1002/esp.1299

Isenko E, Naruse R, Mavlyudov B., 2005. Water temperature in englacial and supraglacial channels: Change along the flow and contribution to ice melting on the channel wall. Cold Regions Science and Technology, **42**(1): 53-62.

Jansson P. 1995. Water pressure and basal sliding on Storglaciären, northern Sweden. Journal of Glaciology **41**: 232-240. DOI: 10.3198/1995JoG41-138-232-240

Jepsen, S.M., Adams, E.E. and Priscu, J.C., 2006. Fuel movement along grain boundaries in ice. Cold Regions Science and Technology, **45**(3): 158-165. DOI:10.1016/j.coldregions.2006.05.005

Jespen SM, Adams EE, Priscu JC. 2010. Sediment melt-migration dynamics in perennial Antarctic lake ice. Arctic, Antarctic, and Alpine Research **42**(1): 57-66. DOI: 10.1657/1938-4246-42.1.57

Karlstrom L, Gajjar P, Manga M. 2013. Meander formation in supraglacial streams. Journal of Geophysical Research: Earth Surface **118**: 1897-1907. DOI: 10.1002/jgrf.20135

Karlstrom L, Zok A, Manga M. 2014. Near-surface permeability in a supraglacial drainage basin on the Llewellyn Glacier, Juneau Icefield, British Columbia. The Cryosphere **8**: 537-546. DOI: 10.5194/tc-8-537-2014

Kestin J, Sokolov M, Wakeham WA. 1978. Viscosity of liquid water in the range− 8 C to 150 C. *Journal of Physical and Chemical Reference Data*, **7**(3): 941-948.

Koizumi K, Naruse R. 1994. Experiments on formation of water channels in a glacier. Journal of the Japanese Society of Snow and Ice **56**: 137-144. DOI: 10.5331/seppyo.56.137

LaChapelle E. 1959. Errors in ablation measurements from settlement and sub-surface melting. Journal of Glaciology **3**: 458-467

Larson GJ. 1977. Internal drainage of stagnant ice: Burroughs Glacier, southeast Alaska. Institute of Polar Studies, Ohio State University.

Larson GJ. 1978. Meltwater storage in a temperate glacier: Burroughs Glacier, Southeast Alaska. Institute of Polar Studies, Ohio State University.

Liestøl O. 1967. Storbreen glacier in Jotunheimen, Norway.

Lliboutry L. 1971. Permeability, brine content and temperature of temperate ice. Journal of Glaciology **10**: 15-29

Lliboutry L. 1996. Temperate ice permeability, stability of water veins and percolation of internal meltwater. Journal of Glaciology **42**(141): 201-211

Łokas E, Zaborska A, Kolicka M, Różycki M, Zawierucha K., 2016. Accumulation of atmospheric radionuclides and heavy metals in cryoconite holes on an Arctic glacier. Chemosphere, **160**: 162-172. DOI: 10.1016/j.chemosphere.2016.06.051

Lu N, Godt JW. 2013. Hillslope hydrology and stability. Cambridge University Press

Mader HM. 1992. Observations of the Water-Vein System in Polycrystalline Ice. Journal of Glaciology **38**: 333-347

Mader HM, Pettitt ME, Wadham JL, Wolff EW, Parkes RJ. 2006. Subsurface ice as a microbial habitat. Geology, **34**(3), pp.169-172.

Mantelli E, Camporeale C, Ridolfi L. 2015. Supraglacial channel inception: Modeling and processes. Water Resources Research **51**: 7044-7063. DOI: 10.1002/2015WR017075

Marsh P, Woo M-K. 1984. Wetting front advance and freezing of meltwater within a snow cover: 1. Observations in the Canadian Arctic. Water Resources Research, **20**(12): 1853-1864.

McGrath D, Colgan W, Steffen K, Lauffenburger P, Balog J. 2011. Assessing the summer water budget of a moulin basin in the Sermeq Avannarleq ablation region, Greenland ice sheet. Journal of Glaciology **57**: 954-964

Miller OL, Solonon DK, Miège C, Koenig L, Forster RR, Montgomery LN, Schmerr N, Ligtenberg S, Legtchenko A, Brucker L., 2017. Hydraulic conductivity of a firn aquifer system in southeast Greenland. Frontiers in Earth Science, **5**: 38. DOI: 10.3389/feart.2017.00038

Mitchell A, Brown GH, Fuge R. 2001. Minor and trace element export from a glacierized Alpine headwater catchment (Haut Glacier d'Arolla, Switzerland). Hydrological Processes **15**: 3499-3524. DOI: 10.1002/hyp.1041

Moore JC, Pälli A, Ludwig F, Blatter H, Jania J, Gadek B, Glowacki P, Mochnacki D, Isaksson E. 1999. High-resolution hydrothermal structure of Hansbreen, Spitsbergen, mapped by ground-penetrating radar. Journal of Glaciology **45**: 524-532. DOI: 10.3198/1999JoG45-151-524-532

Moore JE. 2002. Field hydrogeology: a guide for site investigations and report preparation. Lewis Publishers: New York

Müller F, Keeler CM. 1969. Errors in short term ablation measurement on melting ice surfaces. Journal of Glaciology **8**: 91-105

Munro DS. 1990. Comparison of Melt Energy Computations and Ablatometer Measurements on Melting Ice and Snow. Arctic and Alpine Research **22**: 153-162. DOI: Doi 10.2307/1551300

Munro DS. 2011. Delays of supraglacial runoff from differently defined microbasin areas on the Peyto Glacier. Hydrological Processes, **25**(19): 2983-2994. DOI: 10.1002/hyp.8124

Nye JF. 1991. The rotting of temperate ice. Journal of Crystal Growth **113**: 465-476. DOI: 10.1016/0022-0248(91)90081-F

Oke TR. 1987. Boundary Layer Climates. Routledge: London

Oerlemans J, Giesen RH, van den Broeke MR. 2009. Retreating alpine glaciers: increased melt rates due to accumulation of dust (Vadret da Morteratsch, Switzerland). Journal of Glaciology, **55**(192): 729-736.

Paterson, W.S.B., 1994. The physics of glaciers, Pergamon, 480 pp.

Pavlova PA, Schmid P, Bogdal C, Steinlin C, Jenk TM, Schwikowski M. 2014. Polychlorinated Biphenyls in Glaciers. 1. Deposition History from an Alpine Ice Core. Environmental Science & Technology **48**: 7842-7848. DOI: 10.1021/es5017922

Pellicciotti F, Brock B, Strasser U, Burlando P, Funk M, Corripio J. 2005. An enhanced temperature-index glacier melt model including the shortwave radiation balance: development and testing for Haut Glacier d'Arolla, Switzerland. Journal of Glaciology **51**: 573-587. DOI: 10.3189/172756505781829124

Porter, P.R., Vatne, G., Ng, F. and Irvine-fynn, T.D., 2010. Ice-marginal sediment delivery to the surface of a high-Arctic glacier: Austre Brøggerbreen, Svalbard. Geografiska Annaler, **92A**(4), 437-449.

Rassner, S.M. E., Anesio, A.M., Girdwood, S.E., Hell, K., Gokul, J.K., Whitworth, D.E. and Edwards, A., 2016. Can the Bacterial Community of a High Arctic Glacier Surface Escape Viral Control? Frontiers in Microbiology, **7**, 956. DOI: 10.3389/fmicb.2016.00956

Rennermalm AK, Smith LC, Chu V, Box J, Forster RR, Van den Broeke M, Van As D, Moustafa SE. 2013. Evidence of meltwater retention within the Greenland ice sheet. The Cryosphere **7**: 1433-1445

Reverter F, Li X, Meijer GCM. 2007. Liquid-level measurement system based on a remote grounded capacitive sensor. Sensors and Actuators A, **138**, 1-8

Rippin DM, Pomfret A, King N. 2015. High resolution mapping of supraglacial drainage pathways reveals link between micro-channel drainage density, surface roughness and surface reflectance. Earth Surface Processes and Landforms, **40**(10): 1279-1290. DOI: 10.1002/esp.3719

Ross PJ. 1983. A water level sensor using a capacitance to frequency converter. Journal or Physics E: Scientific Instruments, **16**, 827-828.

Rudolph JV, Friedrich K and Germann U. 2011. Relationship between radar-estimated precipitation and synoptic weather patterns in the European Alps. Journal of Applied Meteorology and Climatology, **50**, 944-957. DOI:10.1175/2010JAMC2570.1

Schneider T. 1999. Water movement in the firn of Storglaciären, Sweden. Journal of Glaciology, **45**(150): 286-294.

Schuster CJ. 2001. Weathering crust processes on melting glacier ices (Alberta, Canada). Wilfred Laurier University; 134pp.

Scott, D., Hood, E. and Nassry, M., 2010. In-stream uptake and retention of C, N and P in a supraglacial stream. Annals of Glaciology, **51**(56): 80-86. DOI

Sharp M, Richards KS, Tranter M. 1998. Introduction. In Glacier hydrology and hydrochemistry, Sharp M, Richards KS, Tranter M (eds.), Wiley, 1-14.

Shumskii P. 1964. Principles of Structural Glaciology: The Petrography of Fresh-Water Ice as a Method of Glaciological Investigation. Dover Publications, New York, USA; 497pp.

Singer GA, Fasching C, Wilhelm L, Niggemann J, Steier P, Dittmar T, Battin TJ. 2012. Biogeochemically diverse organic matter in Alpine glaciers and its downstream fate. Nature Geoscience, **5**(10): 710-714. DOI: 10.1038/ngeo1581

Smart P, Laidlaw I. 1977. An evaluation of some fluorescent dyes for water tracing. Water Resources Research **13**: 15-33

Smith LC, Chu VW, Yang K, Gleason CJ, Pitcher LH, Rennermalm AK, Legleiter CJ, Behar AE, Overstreet BT, Moustafa SE, Tedesco M, Forster RR, LeWinter AL, Finnegan DC, Sheng Y, Balog J. 2015. Efficient meltwater drainage through supraglacial streams and rivers on the southwest Greenland ice sheet. Proceedings of the National Academy of Sciences **112**: 1001-1006. DOI: 10.1073/pnas.1413024112

Smith LC, Yang K, Pitcher LH, Overstreet BT, Chu VW, Rennermalm AK, Ryan JC, Cooper MG, Gleason CJ, Tedesco M, Jeyaratnami J, van As D, van den Broeke MR, van de Berg WJ, Noël B, Langen PL, Cullatherm RI, Zhao B, Willis MJ, Hubbard A, Box JE, Jenner BA, Behar AE. 2017. Direct

measurements of meltwater runoff on the Greenland ice sheet surface. Proceedings of the National Academy of Sciences (early view): 10pp. DOI:10.1073/pnas.1707743114.

St. Germain SL, Moorman BJ. 2016. The development of a pulsating supraglacial stream. Annals of Glaciology **57**: 31-38. DOI: 10.1017/aog.2016.16

Stibal M, Šabacká M, Žárský J., 2012. Biological processes on glacier and ice sheet surfaces. Nature Geoscience, **5**(11): 771-774.

Takeuchi, N., 2002. Optical characteristics of cryoconite (surface dust) on glaciers: the relationship between light absorbency and the property of organic matter contained in the cryoconite. Annals of Glaciology, **34**(1): .409-414.

Theakstone WH, Knudsen NT. 1981. Dye tracer tests of water movement at the glacier Austre Okstindbreen, Norway. Norsk Geografisk Tidsskrift **35**: 21-28. DOI: 10.1080/00291958108621970

van de Wal RSW, Boot W, van den Broeke MR, Smeets CJPP, Reijmer CH, Donker JJA, Oerlemans J. 2008. Large and Rapid Melt-Induced Velocity Changes in the Ablation Zone of the Greenland Ice Sheet. Science **321**: 111-113. DOI: 10.1126/science.1158540

van de Wal RSW, Greuell W, van den Broeke MR, Reijmer CH, Oerlemans J. 2005. Surface mass-balance observations and automatic weather station data along a transect near Kangerlussuaq, West Greenland. Annals of Glaciology **42**: 311-316. DOI: 10.3189/172756405781812529

Wainstein P, Moorman B, Whitehead K. 2014. Glacial conditions that contribute to the regeneration of Fountain Glacier proglacial icing, Bylot Island, Canada. Hydrological Processes **28**: 2749-2760. DOI: 10.1002/hyp.9787

Wakahama G. 1978. Observations of the melt-water permeation in the near-surface ice layers of the Mendenhall Glacier, south-east Alaska. Mater. Glyatsiologicheskogo Issled. Khronika Obsuzhdeniya **33**: 175-178

Wakahama G, Kuroiwa D, Kobayashi D, Tanuma K, Endo Y, Mizuno Y, Kobayashi S. 1973. Observations of permeating water through a glacier body. Low Temperature Science A **31**: 217-219

Whitehead K, Moorman BJ, Hugenholtz CH. 2013. Brief Communication: Low-cost, on-demand aerial photogrammetry for glaciological measurement. The Cryosphere **7**: 1879-1884. DOI: 10.5194/tc-7-1879-2013

Whitehead K, Moorman BJ, Wainstein P. 2014. Measuring daily surface elevation and velocity variations across a polythermal arctic glacier using ground-based photogrammetry Journal of Glaciology **60**: 1208-1220. DOI: 10.3189/2014JoG14J080

Willis IC, Arnold NS, Brock BW. 2002. Effect of snowpack removal on energy balance, melt and runoff in a small supraglacial catchment. Hydrological Processes **16:** 2721-2749. DOI: 10.1002/hyp.1067

Wilhelm L, Singer GA, Fasching C, Battin TJ, Besemer K. 2013. Microbial biodiversity in glacier-fed streams. ISME Journal, **7**(8): 1651-1660. DOI:10.1038/ismej.2013.44

Wilner LB. 1960. Variable capacitance liquid level sensor. Review of Scientific Instruments, **31**, 501-507.

Yang K, Karlstrom L, Smith LC, Li M. 2016. Automated High-Resolution Satellite Image Registration Using Supraglacial Rivers on the Greenland Ice Sheet. IEEE Journal of Selected Topics in Applied Earth Observations and Remote Sensing, **10**(3): 845-856.

Yang K, Smith LC. 2013. Supraglacial streams on the Greenland Ice Sheet delineated from combined spectral–shape information in high-resolution satellite imagery. IEEE Geoscience and Remote Sensing Letters **10**: 801-805

Younger, P.L., 2009. Groundwater in the environment: an introduction. John Wiley & Sons.

Zeng Q, Cao M, Feng X, Liang F, Chen X, Sheng W. 1984. A study of spectral reflection characteristics for snow, ice and water in the north of China. Hydrological applications of remote sensing and remote data transmission **145**: 451-462

Table I. Summary of glacier sites sampled within the study. Daylight hours and solar zenith ranges are reported for the fieldwork period.

Glacier Name	Country	Fieldwork Period	Glacier Code	Latitude (°N)	Area (km^2)	Elevation (m asl)	Daylight hours (decimal)	Max daily solar zenith (°)	Climate and thermal regime	Further reference
Protektorbreen	Svalbard, Norway	13/08/2015 – 17/08/2015	PBSV	78.24	7.60	5 – 700	24	25.2 – 26.5	Polar maritime Cold	(Hagen*, et al.*, 1993; Hodson and Irvine-Fynn, unpublished data)
Foxfonna	Svalbard, Norway	08/08/2015	FFSV	78.12	3.95	675 – 950	24	28.0	Polar maritime Cold	(Hagen*, et al.*, 1993, Liestøl, 1967, Rutter*, et al.*, 2011)
Fountain Glacier	Bylot Island, Canada	08/07/2014 – 23/07/2014	FGBI	72.96	72.0	330 – 1100	24	37.2 – 39.5	Polar continental Non-temperate polythermal	(St. Germain and Moorman, 2016, Wainstein*, et al.*, 2014, Whitehead*, et al.*, 2013, Whitehead*, et al.*, 2014)
Rabots Glaciär	Sweden	22/08/2014	RGSE	67.91	3.70	1070 – 1640	16.4	33.8	Polar maritime Non-temperate polythermal	(Björnsson, 1981, Brugger, 2007, Brugger*, et al.*, 2005)
Storglaciären	Sweden	24/08/2014	SGSE	67.90	3.10	1120 – 1730	16.1	33.1	Polar maritime Non-temperate	(Björnsson, 1981, Brugger, 2007, Hock and Holmgren, 2005, Holmlund and Eriksson, 1989, Jansson, 1995)
Greenland Ice Sheet (Point 660)	Greenland	06/08/2014 – 07/08/2014	GRKM	67.16	N/A	~630	18.2 – 18.3	39.6 – 39.9	Polar maritime Non-temperate	(Smith*, et al.*, 2015, van de Wal*, et al.*, 2008, van de Wal*, et al.*, 2005, Yang*, et al.*, 2016)
Greenland Ice Sheet (S6)	Greenland	22/07/2014 – 29/07/2014	GRDS	67.08	N/A	~1100	19.5 – 20.6	41.9 – 43.4	Polar maritime Non-temperate	
Gaisbergferner	Austria	08/09/2014	GBOS	46.83	1.03	2460 – 3390	12.9	48.8	Alpine continental Temperate	(Abermann*, et al.*, 2009, Fischer, 2010)

Rotmoosferner	Austria	11/09/2014	RMOS	46.82	3.17	2450 – 3000	12.9	47.6	Alpine continental Temperate	(Abermann*, et al.*, 2009, Anesio*, et al.*, 2010, Edwards*, et al.*, 2013)
Haut Glacier d'Arolla	Switzerland	19/07/2015 – 28/07/2015	HACH	45.98	6.30	2550 – 3500	14.9 – 15.3	63.0 – 64.5	Alpine Temperate	(Brock*, et al.*, 2000, Mitchell*, et al.*, 2001, Pellicciotti*, et al.*, 2005, Willis*, et al.*, 2002)

Table II. Correlation matrix highlighting monotonic relationships with hypothesised controls upon hydraulic conductivity (*K*) of the weathering crust. Values shown are Spearman's *r* with significant values (two-tailed) marked: p<0.05*, p<0.01**. Sample number, n, is indicated in brackets for instances indicated by # with missing cases or lacking data.

Glacier	n	Cum. SWR_{in} 0°C	Cum. SWR_{in} Precip	Cum. SWR_{in} DTEF	Elevation	Water Table	Melt
PBSV	54	0.398**	-	-	-0.321*	0.547**	0.520**
FFSV	9	-	-	-	-	0.786*	-
FGBI	40	0.281	-	-	0.173	0.375*	-
RGSE	12	0.272	0.272	0.272	0.203	0.835**	-0.488
SGSE	31	-0.050	-0.050	-0.050	0.428*	0.249	0.212
GRDS	40#	0.209	-	-0.133 (30)	0.123	0.639**	0.225
GRKM	23	-	-	-	-	0.352	-
GBOS	7	-	-	-	-0.40	0.809*	-
RMOS	7	-	-	-	-0.378	-0.204	-
HACH	57#	0.098	0.112 (19)	-	0.168	0.306*	-0.253
All	280#	-0.404** (234)	0.134 (62)	-0.658** (73)	-0.256**	0.710**	-0.52 (129)

Table III. Correlation matrix highlighting monotonic relationships with hypothesised controls upon permeability (κ) of the weathering crust. Values shown are Spearman's *r* with significant values (two-tailed) marked as thus: p<0.05*, p<0.01**. Latitude is not considered as independent variables due to a lack of data.

Glacier	n	Cum. SWR_{in}	Elevation	Water Table	Melt
PBSV	54	0.398**	-0.321*	0.548*	0.519**
HACH	57	0.093	0.171	0.304*	-0.272
All	111	-0.165	-0.291**	0.574**	0.415**

.

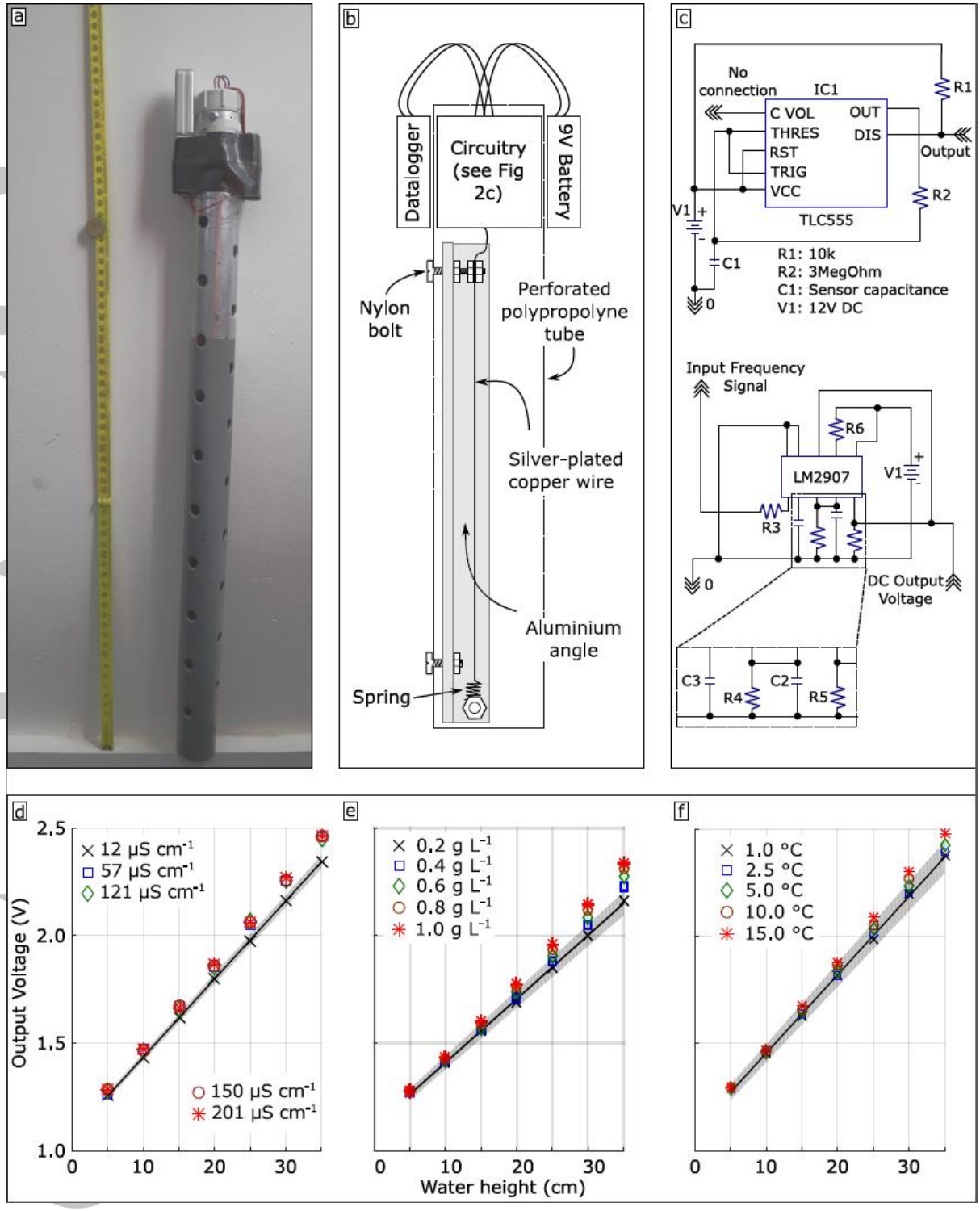

Figure 1. Probe design and calibration: (a) image of a water-level probe including a centimetre scale; (b) cartoon schematic of the probe design; and (c) wiring diagram for the probe circuitry. Probe voltage outputs at given water levels under specific water conditions, for the typical supraglacial conditions (X) and for other variable conditions of electrical conductivity (d), suspended sediment load (e) and temperature (f), with the black line indicating a linear regression ($r^2 > 0.99$) and the greyed area reflecting the 95% confidence bound.

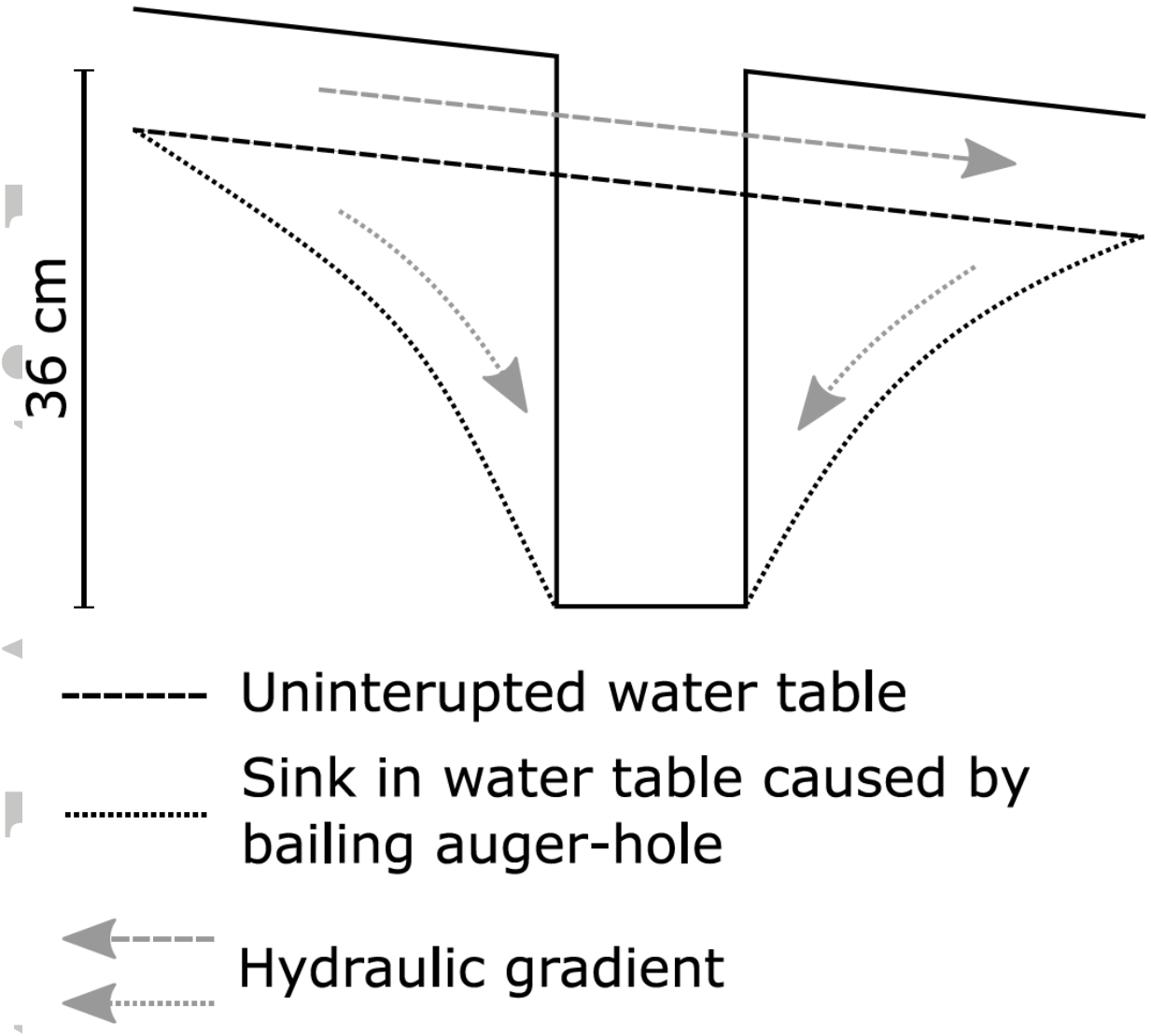

Figure 2. The role of auger-hole drilling on the water table and idealised hydraulic head. The drilling and bailing of an auger hole causes a localised drop in the water table (with radius up to 2 m) altering the hydraulic gradient. Note that the hydraulic gradient indicated corresponds with the water table of the same line style.

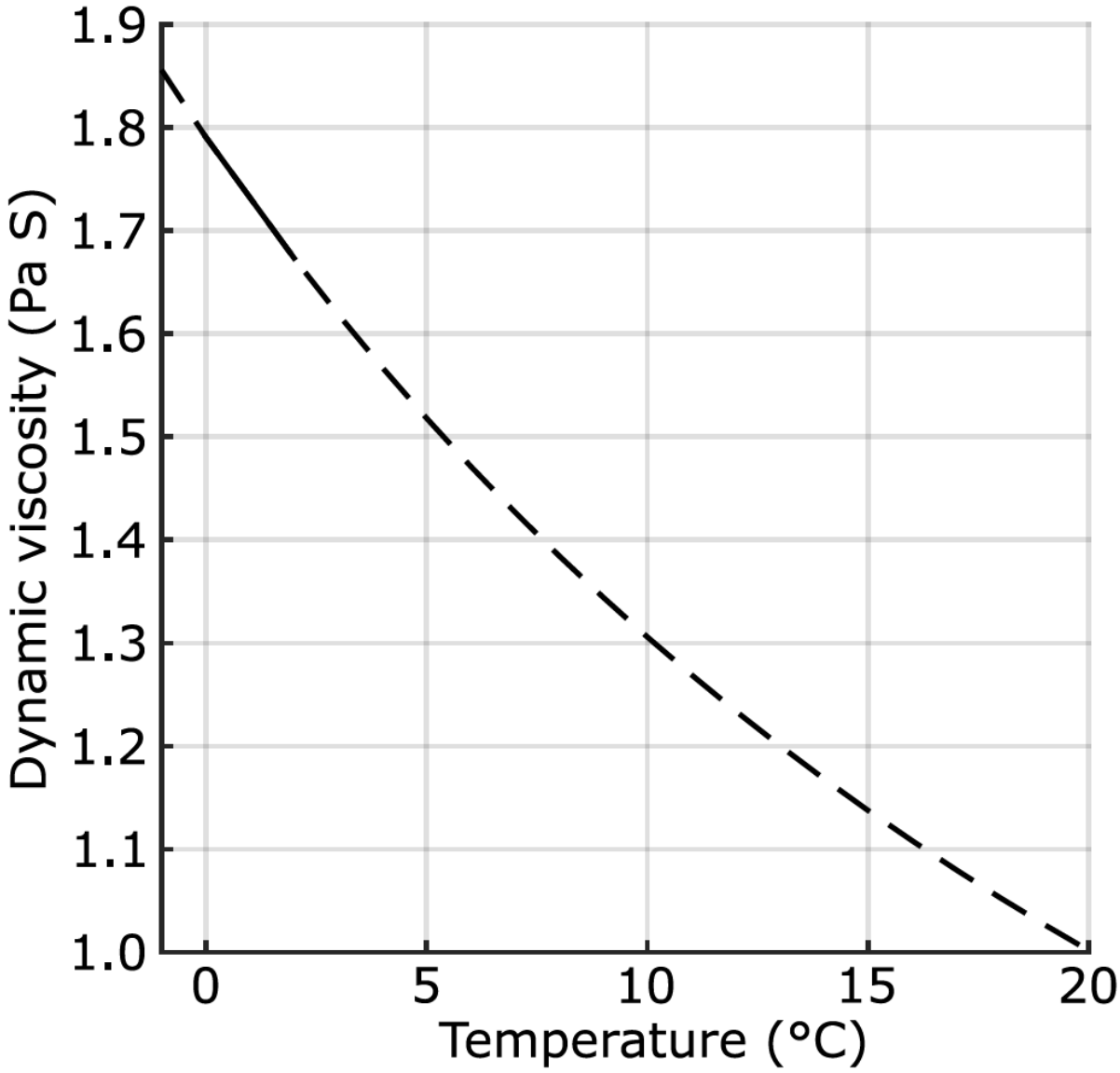

Figure 3. Dynamic viscosity, μ, of water as controlled by temperature in the range -1 °C ≥ t ≥ 20 °C (after Kestin et al, 1978). Note, the area of interest, 0.1 °C ≥ t ≥ 2 °C, aligning with observed auger-hole temperatures, is highlighted with a solid line.

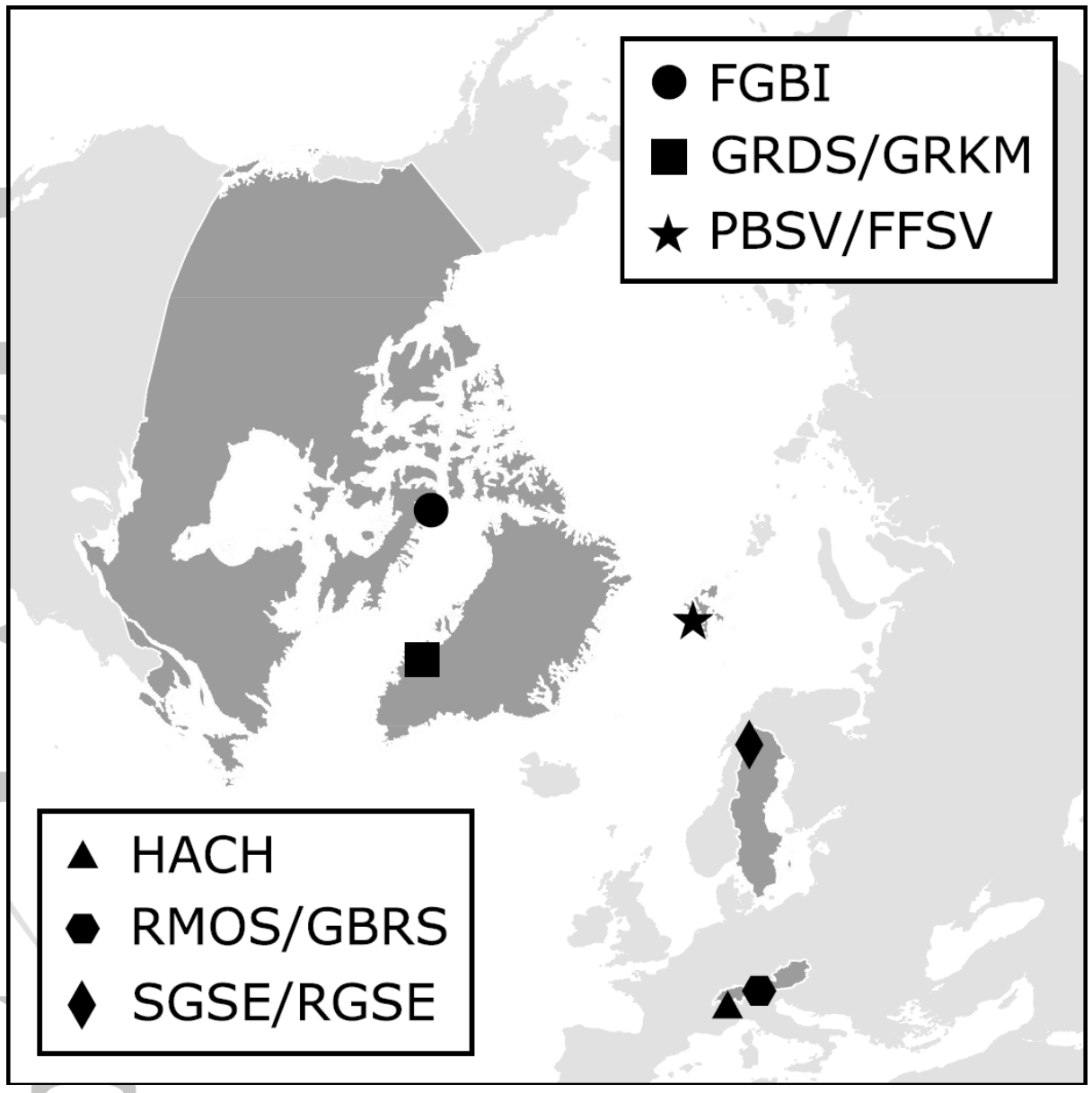

Figure 4. A hemispheric location map of glaciers sampled within this study. Letter codes are identified within Table I.

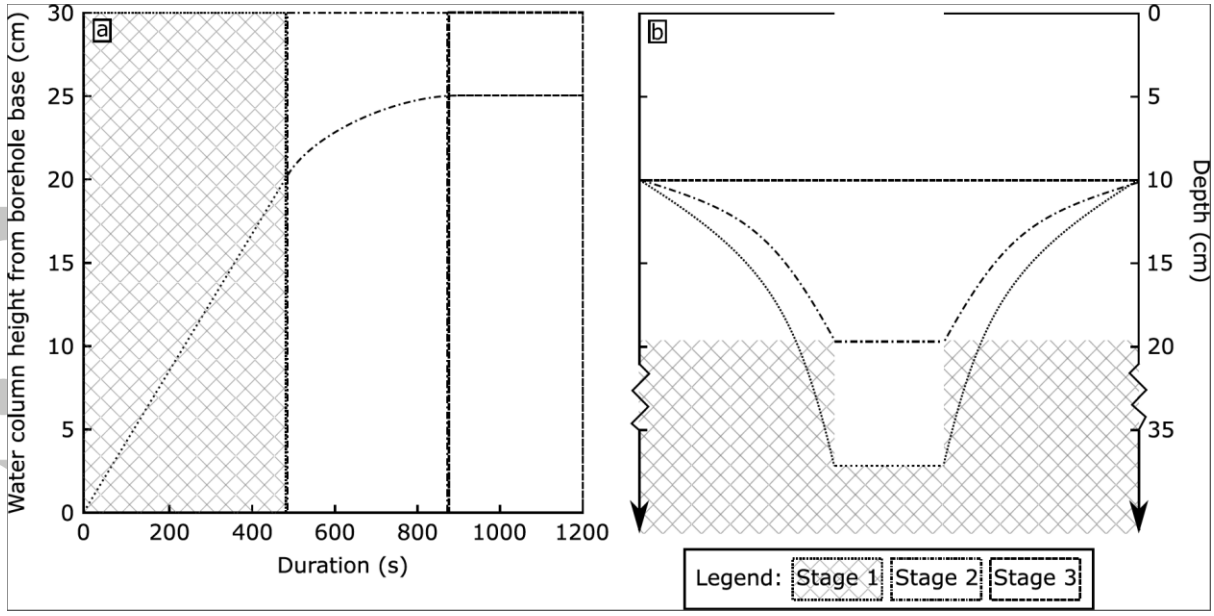

Figure 5. (a) An idealised recharge curve related to a schematic cross-section of the auger-hole (b). In panel (b) each dashed line indicates the position of an idealised water table; during Stage 1, anisotropic, pressure driven flow dominates due to the large hydraulic head generated by the presence of an auger-hole (in black) generated sink in the water table. Through Stage 2, this influence is reduced (although still prevalent) but influence of this false water head decreases as the hole fills (aligning with the non-linear stage in panel (i). At Stage 3, the water level in the borehole is equilibrated with the surrounding water table and recharge stops as the auger-hole becomes equilibrated with the surrounding weathering crust water table.

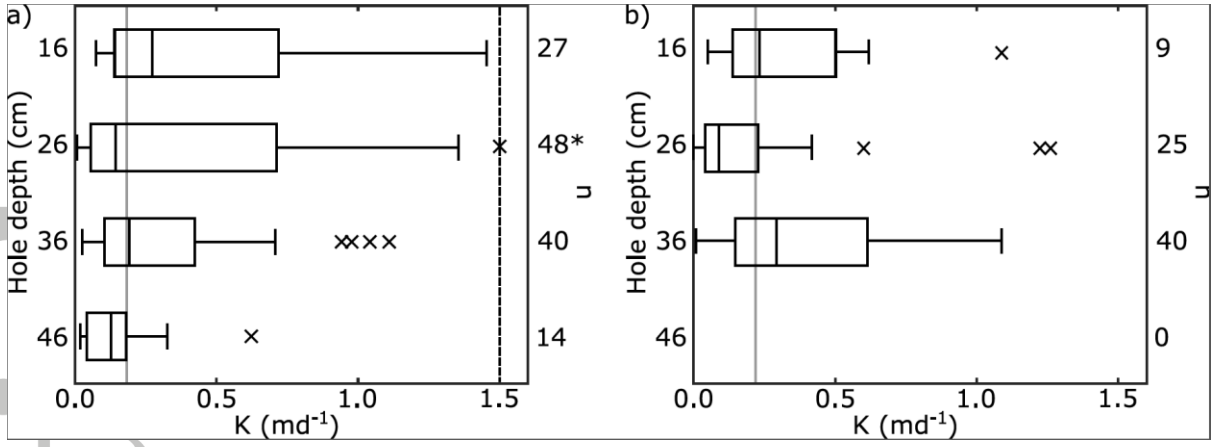

Figure 6. change in K with auger-hole depth for (a) FGBI and (b) GRDS, indicating median for each site (solid vertical line) of 0.183 and 0.220 m d^{-1}, respectively. Sample sizes (n) are noted on the right of the diagram. *Note one outlying data point > 1.5 m d^{-1}.

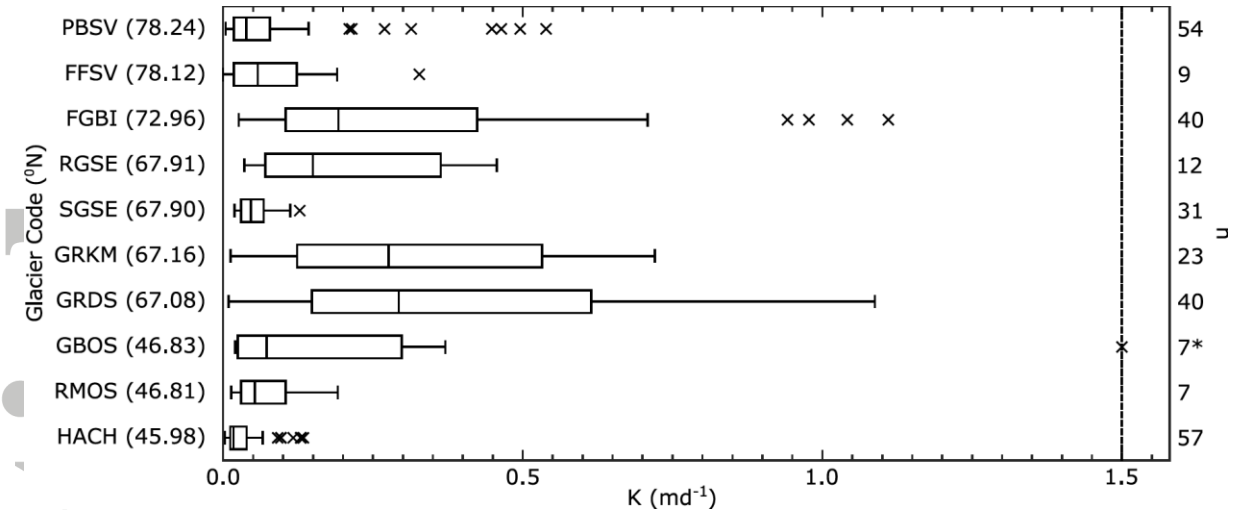

Figure 7. Box-and-whisker plot showing hydraulic conductivity of holes of 36 cm depth across all glaciers within the sample set, with latitudes displayed in degrees North of the equator. Sample sizes (n) are noted on the right of the diagram. *Note, the x axis is limited to 1.5 m d^{-1}, with one outlying point above this limit at GBOS, with a value of 3.519 m d^{-1}.